Dynamics of TGF-β signaling reveal adaptive and pulsatile behaviors reflected in the nuclear localization of transcription factor Smad4

Aryeh Warmflash[a,b], Qixiang Zhang[b], Benoit Sorre[a,b], Alin Vonica[b,1], Eric D. Siggia[a,2], and Ali H. Brivanlou[b,2]

[a]Center for Studies in Physics and Biology and [b]Laboratory for Molecular Vertebrate Embryology, The Rockefeller University, New York, NY 10065

Contributed by Eric Dean Siggia, May 7, 2012 (sent for review March 26, 2012)

The TGF-β pathway plays a vital role in development and disease and regulates transcription through a complex composed of receptor-regulated Smads (R-Smads) and Smad4. Extensive biochemical and genetic studies argue that the pathway is activated through R-Smad phosphorylation; however, the dynamics of signaling remain largely unexplored. We monitored signaling and transcriptional dynamics and found that although R-Smads stably translocate to the nucleus under continuous pathway stimulation, transcription of direct targets is transient. Surprisingly, Smad4 nuclear localization is confined to short pulses that coincide with transcriptional activity. Upon perturbation, the dynamics of transcription correlate with Smad4 nuclear localization rather than with R-Smad activity. In *Xenopus* embryos, Smad4 shows stereotyped, uncorrelated bursts of nuclear localization, but activated R-Smads are uniform. Thus, R-Smads relay graded information about ligand levels that is integrated with intrinsic temporal control reflected in Smad4 into the active signaling complex.

quantitative live-cell imaging | signaling dynamics | TGF-β signaling | *Xenopus* development | adaptation

A small number of signaling pathways are used repeatedly throughout metazoan development, and their effects depend upon timing and context (1). Extensive biochemical characterization of these developmental signaling pathways has elucidated the sequence of events leading from ligand binding at the cell surface to regulation of transcription. Proper temporal control of pathway activity is crucial for normal development; however, the dynamic aspects of signaling are difficult to infer from population data and have lagged behind dissection of pathway components (2, 3). The few cases that have been examined have revealed rich dynamics that could not have been predicted from knowledge of the molecular interactions or from bulk measurements of protein modifications or mRNA levels (2–4).

The TGF-β pathway is essential for developmental processes including mesoderm specification and dorsal–ventral axis formation and is dysregulated in a variety of cancers. It also is an important model for pathway crosstalk and dynamics, because it has two branches that share several components including receptors and transcription factors (5, 6). Binding of ligands specific to each branch to receptor complexes leads to the phosphorylation of branch-specific transcription factors: TGF-β/activin/nodal ligands induce the phosphorylation of Smad2/3, whereas bone morphogenic proteins (BMPs) activate Smad1/5/8. Phosphorylation of the receptor-activated Smads (R-Smads) from either branch of the pathway results in complex formation with Smad4, nuclear accumulation, and transcriptional activation.

The prevailing model is that R-Smads carry pathway information with Smad4 mirroring their activity (7, 8). R-Smad phosphorylation is necessary for the nuclear accumulation and transcriptional activity of both the R-Smads and Smad4. Termination of signaling often is presumed to be caused by either degradation or dephosphorylation of activated R-Smads (9, 10), and it further is assumed that the continuous presence of activated R-Smads is synonymous with continuous transcriptional activity. We reexamine these issues here using dynamic measurements. We show that R-Smad phosphorylation and nuclear accumulation stably reflect the ligand level to which the cells are exposed; however, both nuclear Smad4 and transcriptional activity show an adaptive response, pulsing in response to changing ligand concentration and then returning to near-baseline levels. These results show that transcriptional dynamics are governed predominantly by feedback reflected in Smad4 but not receptor or R-Smad dynamics and force a substantial revision of the conventional view about a pathway ubiquitous in development and disease.

Results

Nuclear Smad2 Levels Stably Reflect the External Ligand Concentration. To observe the dynamic response of Smad2 in single cells, we used the ePiggyBac transposable element system (11) to generate a clonal cell line of mouse myoblast C2C12 cells stably expressing an RFP-Smad2 fusion protein (Fig. 1*A*). These cells also stably express GFP-nuclear localization signal (NLS) to allow automated identification and tracking of cells using custom software. Western blot analysis revealed that RFP-Smad2 is expressed at levels close to that of endogenous Smad2 and is phosphorylated (denoted hereafter "pSmad2") at its C terminus in response to signal (compare Fig. S1*A* and Fig. 1*F*), and quantitative RT-PCR (qRT-PCR) analysis showed similar induction of TGF-β target genes upon ligand stimulation in the modified cell line as compared with the parental cell line (compare Fig. S1*B* and Fig. 2*B*). RFP-Smad2 accumulated in the nucleus in response to stimulation with TGF-β1 (Fig. 1*B*). Continued nuclear localization of Smad2 was dependent on continuous signaling, because the addition of SB431542, a specific inhibitor of type I TGF-β receptors (12), 1 h after stimulation caused nuclear fluorescence to return to below the starting baseline within 4 h (Fig. 1*C*). Thus, RFP-Smad2 is a reliable reporter for the activation status of Smad2, accumulating in the nucleus when the pathway is stimulated with ligand and returning to the cytoplasm upon pathway inhibition.

We used the RFP-Smad2 cell line to assess the response of single cells to varying doses of TGF-β1 ligand. In contrast to other signaling pathways such as NFκB that display binary on/off responses (3), essentially all cells responded to ligand at both high and low doses. The response was graded, with increasing TGF-β1 concentration resulting in increasing nuclear RFP-Smad2 (Fig. S1*C*). At

Author contributions: A.W., B.S., A.V., E.D.S., and A.H.B. designed research; A.W., Q.Z., and B.S. performed research; A.W. and E.D.S. analyzed data; and A.W., E.D.S., and A.H.B. wrote the paper.

The authors declare no conflict of interest.

[1]Present Address: Department of Biomedical Genetics, University of Rochester Medical Center, Rochester, NY 14642.

[2]To whom correspondence may be addressed. E-mail: siggiae@rockefeller.edu or brvnlou@rockefeller.edu.

See Author Summary on page 11076 (volume 109, number 28).

This article contains supporting information online at www.pnas.org/lookup/suppl/doi:10.1073/pnas.1207607109/-/DCSupplemental.

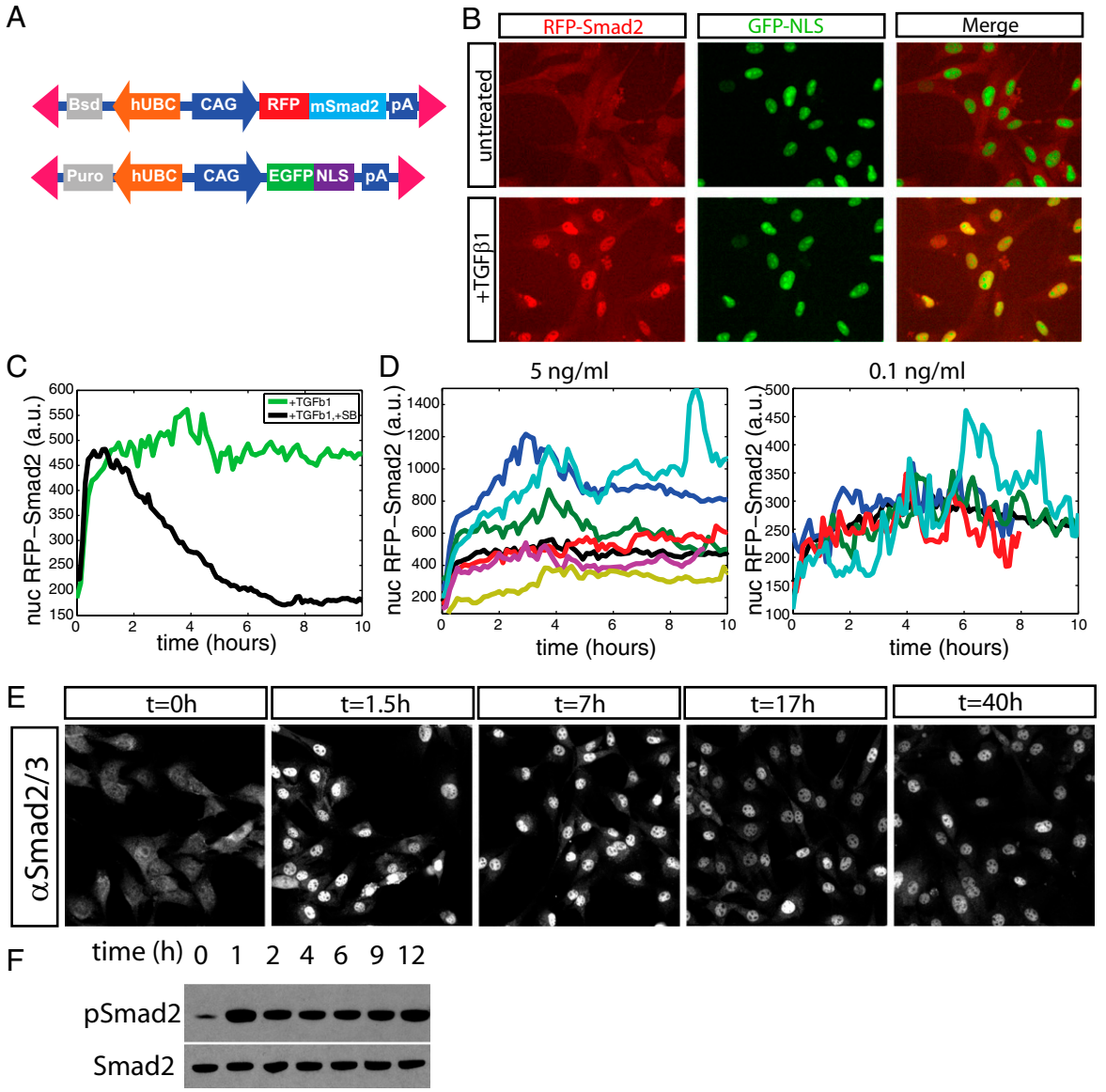

Fig. 1. Smad2 activation is stable under continuous stimulation. (*A*) Constructs used to generate the RFP-Smad2 cell line. Triangles denote the ePiggyBac terminal repeats, arrows denote promoters, and gray boxes denote antibiotic resistance genes. (*B*) Images of live untreated cells (*Upper*) or cells treated with 5 ng/mL TGF-β1 for 1 h (*Lower*) showing accumulation of RFP-Smad2 in the nucleus upon TGF-β1 treatment. (*C*) Quantification of average nuclear RFP-Smad2 from live cell imaging in cells exposed first to 5 ng/mL TGF-β1 and then exposed to 10 uM SB431542 1 h later, showing that pathway inhibition results in relocalization of RFP-Smad2 to the cytoplasm (*D*) Time courses of nuclear RFP-Smad2 show stable nuclear accumulation in cells exposed to either high (5 ng/mL) or low (0.1 ng/mL) doses of TGF-β1. Black lines represent averages of all cells in the field of view (>50 cells). Colored lines represent selected single cells. Cell nuclei were identified automatically and tracked through time using the GFP-NLS nuclear marker. (*E*) Immunofluorescent staining for Smad2/3 at the indicated times after continuous application of 1 ng/mL TGF-β1 showing stable enrichment of endogenous Smad2/3 in the nucleus. (*F*) Western blots of total cell lysates from cells continuously exposed to 5 ng/mL TGF-β1 for the indicated times show stably elevated pSmad2/3 levels.

the level of single cells, this response resulted in a rightward shift in the histogram of nuclear RFP-Smad2 values, but the distribution remained single peaked (Fig. S1*D*). At doses greater than 1 ng/mL, the response saturated, with RFP-Smad2 exclusively nuclear and all cells responding. We used time-lapse imaging to determine the dynamic response of Smad2 to stimulation with both high and low doses of ligand in individual cells (Fig. 1*D* and Movie S1). In both cases, response to ligand was detectable within 10 min and peaked at 1–2 h. Consistent with the results shown in Fig. S1*D*, nearly all cells responded at both high and low ligand doses. We found that nuclear enrichment of RFP-Smad2 was extremely long lived and lasted for the entire duration of the movie (at least 12 h) at both high and low ligand doses.

We confirmed these results by detecting endogenous Smad2/3 in the parental cell line by immunofluorescence (Fig. 1*E*). Nuclear accumulation of endogenous Smad2/3 occurred in a graded fashion in response to ligand stimulation (Fig. S1*E*) and was very long lived (Fig. 1*E*). Smad2/3 still was almost exclusively nuclear after 40 h of continuous stimulation with some reduction in intensity compared with 1.5 h, likely because of preferential degradation of phosphorylated Smad2 (13, 14). Consistent with the continuous presence of Smad2/3 in the nucleus, Western blotting revealed that cells continuously exposed to ligand had high levels of pSmad2/3 at all time points examined (up to 12 h) (Fig. 1*F*). We obtained similar results in the HaCaT cell line (Fig. S1 *F* and *G*). Taken together, our results imply that Smad2/3 activation

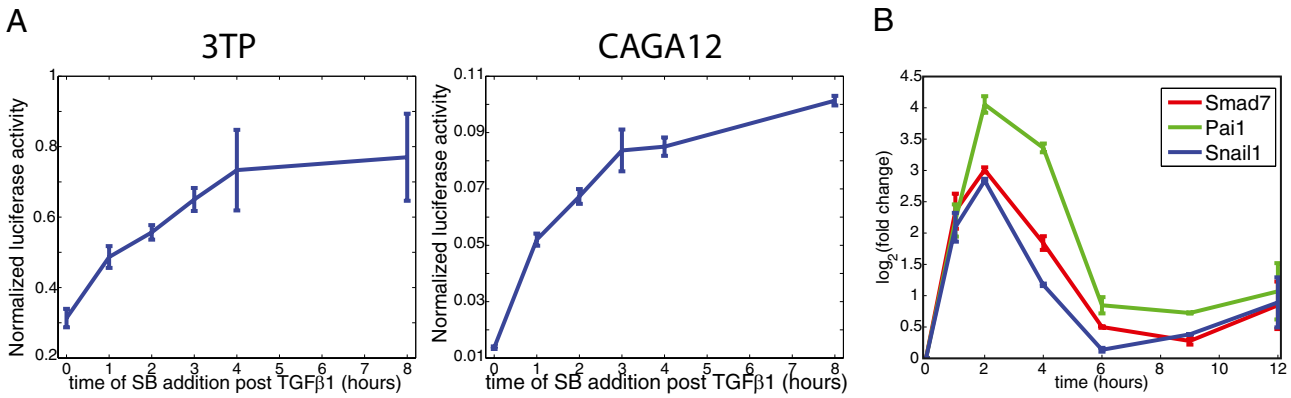

Fig. 2. TGF-β–mediated transcriptional responses adapt under continuous stimulation. (*A*) Production of luciferase from TGF-β–sensitive reporters is limited to the first 3–4 h following stimulation. C2C12 Cells were transiently transfected with the CAGA12 or 3TP constructs. Forty-eight hours after transfection cells were treated with TGF-β and then with SB431542 at the indicated times after the addition of TGF-β. After 8 h, all samples were collected together and analyzed for luciferase activity. Activity of the TGF-β reporters was normalized using constitutive Renilla expression from the pRL-Tk plasmid. (*B*) Expression of TGF-β target genes by qRT-PCR as a function of time after TGF-β1 treatment showing a transient response to continuous TGF-β1 stimulation.

stably reflects the level of ligand to which cells are exposed and will rise and fall with the levels of receptor activation.

Transcriptional Response to TGF-β Is Adaptive. Given that Smad2 exhibits stable nuclear accumulation upon continuous TGF-β1 stimulation (Fig. 1 *D* and *F*), we asked whether the dynamics of TGF-β1–dependent transcription are sustained similarly. We first examined transcription from CAGA12 and 3TP synthetic luciferase reporters. CAGA12 is a reporter construct containing 12 copies of the Smad-binding element known as a "CAGA box" (15), whereas the 3TP reporter contains a 105-bp TGF-β–inducible element from the human Pai-1 promoter (16). To follow the kinetics of signaling, we stimulated cells with TGF-β1 and then added SB431542 at variable times after stimulation (17). Because luciferase is stable over the time scale of the experiment, the luciferase activity should continue to increase as long as the signaling pathway is active. The time point at which addition of the inhibitor no longer affects the final luciferase activity is also the time point at which the signaling pathway is no longer active. Surprisingly, and in contrast to our results for Smad2, we found that for both reporters most signaling-dependent transcription occurred within the first 2 h and that adding the inhibitor at 4 h had little or no effect (Fig. 2*A*). This outcome suggests that, despite the continuously elevated levels of nuclear, activated Smad2/3, transcriptional activity returns to baseline levels within 4 h.

We also examined the kinetics of endogenous target gene (18) expression by qRT-PCR in unmodified C2C12 cells. The response of all three target genes we studied was transient, rising over the first 2 h after stimulation and returning to baseline within 4–6 h (Fig. 2*B*). The dynamics of transcription in the RFP-Smad2 cells are very similar to those of the unmodified cell line (Fig. S1*B*). Thus, both luciferase reporter and qRT-PCR assays support a window of ∼4 h for TGF-β–dependent transcription under continuous ligand stimulation. The discrepancy between the dynamics of nuclear activated Smad2 and transcription was surprising, because activated R-Smads in the nucleus typically are assumed to indicate that the pathway is active. We reasoned that the short-lived transcription may result from the transient activity of other pathway components and sought to determine the status of the R-Smad binding partner Smad4, which is required for TGF-β–mediated transcriptional responses.

Smad4 Response Is Transient and Coincides with Transcription. To monitor the dynamics of Smad4 in single living cells, we created a clonal C2C12 cell line expressing a GFP-Smad4 fusion protein as well as unlabeled Smad2 to enhance the Smad4 response (8, 19) and an RFP-H2B fusion protein for automated cell identification and tracking (Fig. 3*A*). Smad2 expression was similar to that in the RFP-Smad2 cell line (Fig. S2 *B* and *C*), and Smad2 phosphorylation (Fig. S2*A*) and nuclear accumulation (Fig. S2*D*) were similar to that in the parental cell line. Importantly, the dynamics of TGF-β target gene induction were nearly identical to those in unmodified C2C12 cells (compare Fig. 2*B* and Fig. S2*E*). Under continuous TGF-β1 stimulation, Smad4 accumulated rapidly in the nucleus of nearly every cell (Fig. 3*B* and Movie S2). Surprisingly, however, we found that, in contrast to Smad2, after the initial burst of nuclear localization, Smad4 relocalized to the cytoplasm after 4 h of continuous TGF-β1 stimulation (Fig. 3 *B–D* and Movie S2). Quantification of nuclear fluorescence in single cells confirmed that all cells had returned to near-baseline values within 4 h (Fig. 3*C*). Thus, the timing of the transcriptional response coincides with Smad4 but not Smad2 nuclear accumulation (Fig. 3*D*).

The kinetics of the Smad4 pulse were not dependent on ligand dose, because cells treated with high (5 ng/mL) and low (0.1 ng/mL) doses of TGF-β1 produced pulses of the same duration but different amplitudes (Fig. 3*E*). These kinetics also were not dependent on continuous signaling from the receptor. Withdrawal of the ligand or treatment of cells with SB431542 1 h after TGF-β1 stimulation had little effect on the kinetics of the pulse and affected only the baseline level to which signaling returned (Fig. 3*F*). The dynamics of the Smad4 pulse are not particular to the levels of Smad expression in our cell line, because the dynamics of all responding cells in the polyclonal cell line from which the clonal line was selected were nearly identical. These results show that Smad4 undergoes stereotyped pulses of nuclear localization whose timing does not depend on ligand dose or on the duration of stimulation.

We sought to confirm these results by detecting endogenous Smad4 by immunofluorescence in the parental C2C12 cell line; however, all antibodies tested showed either weak or nonspecific staining. Immunofluorescent analysis of Smad4 in HaCaT cells revealed that in dense cultures Smad4 uniformly shifted to the nucleus in response to TGF-β1 treatment and then returned to baseline within 4 h, paralleling the time course in C2C12 cells (Fig. S2 *F* and *H*). Fractionating the nuclear and cytoplasmic compartments in dense cultures of HaCaT cells also revealed transient responses for Smad4 and sustained responses for Smad2 (Fig. S2*I*). Interestingly, in low-density cultures, nuclear localization was heterogeneous, and treatment with TGF-β1 did not synchronize the cells; Smad4 remained heterogeneous (Fig. S2*G*). Smad4 nuclear localization in both cases was caused by

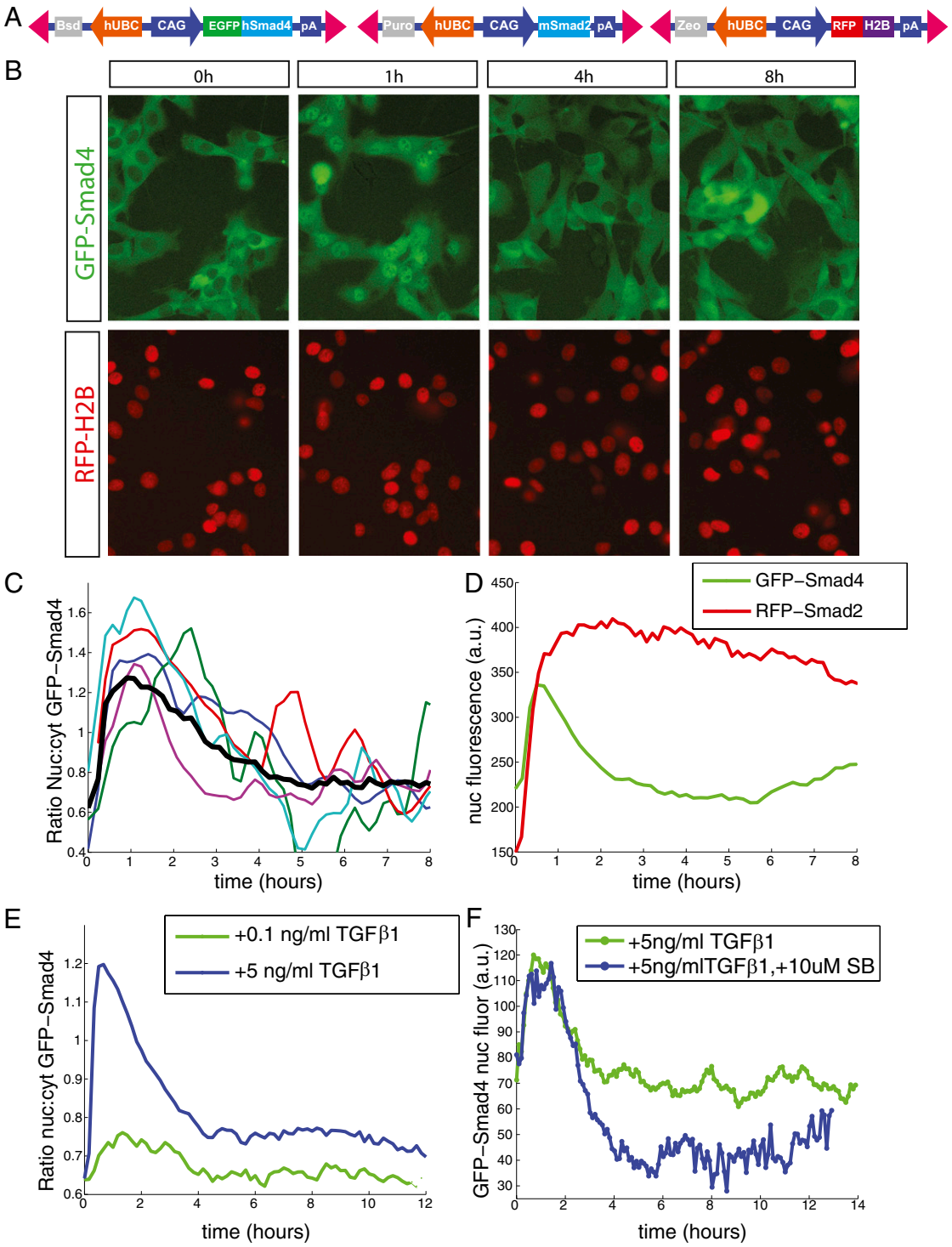

Fig. 3. Smad4 adapts to a step in ligand concentration, and Smad4 nuclear localization coincides with transcription. (*A*) Constructs used in generating the Smad4 cell line. Notation is as in Fig. 1*A*. (*B*) Snapshots from a time-lapse movie of cells exposed to 5 ng/mL TGF-β1 at time t = 0. Smad4 is enriched in the nucleus after 1 h but becomes mostly cytoplasmic by 4 h. (*C*) Quantification of single-cell trajectories (colored lines) and average trajectory (black line). (*D*) Comparison of average RFP-Smad2 and GFP-Smad4 fluorescence in the nucleus as a function of the duration of continuous TGF-β1 treatment. Smad2 nuclear accumulation is sustained, whereas Smad4 is transient. (*E*) Smad4 amplitude but not kinetics is dependent on the dose of TGF-β1 ligand. Comparison of average nuclear to cytoplasmic GFP-Smad4 in cells treated with either 0.1 or 5 ng/mL TGF-β1. (*F*) Smad4 kinetics does not require continuous signaling. C2C12 GFP-Smad4 Cells were treated with 5 ng/mL TGF-β1 only or with 5 ng/mL TGF-β1 and then with 10 μM SB431542 1 h later. Traces show average nuclear fluorescence as a function of time.

TGF-β signaling, because it was prevented by treatment with SB431542. These results should be contrasted with those for Smad2 in HaCaT cells, which showed long-lived, uniform nuclear accumulation in response to TGF-β1 in both low- and high-density cultures (Fig. S1). Based on the heterogeneity of Smad4 localization in sparse cultures of HaCaT cells, we speculate that

under these conditions Smad4 may show repeated asynchronous pulses of nuclear localization similar to those observed in the *Xenopus* embryo (see below).

Relocalization of Smad4 to the Cytoplasm Is Dependent on New Protein Synthesis. We next investigated whether negative feedback dependent on new protein synthesis is required for the removal of Smad4 from the nucleus in C2C12 cells. Consistent with this hypothesis, treatment with the protein synthesis inhibitor cycloheximide greatly prolonged the time that GFP-Smad4 spends in the nucleus under continuous TGF-β1 stimulation (Fig. 4 *A* and *B* and Movie S3).

We used the RFP-Smad2 cell line to determine the effects of cycloheximide on Smad2 dynamics. In agreement with previous results (17), the amount of Smad2 in the nucleus decreased more in cells treated with TGF-β1 and cycloheximide than in cells treated with TGF-β1 alone (Fig. 4*C*). When cells were treated with cycloheximide and TGF-β1, RFP-Smad2 accumulated nor-

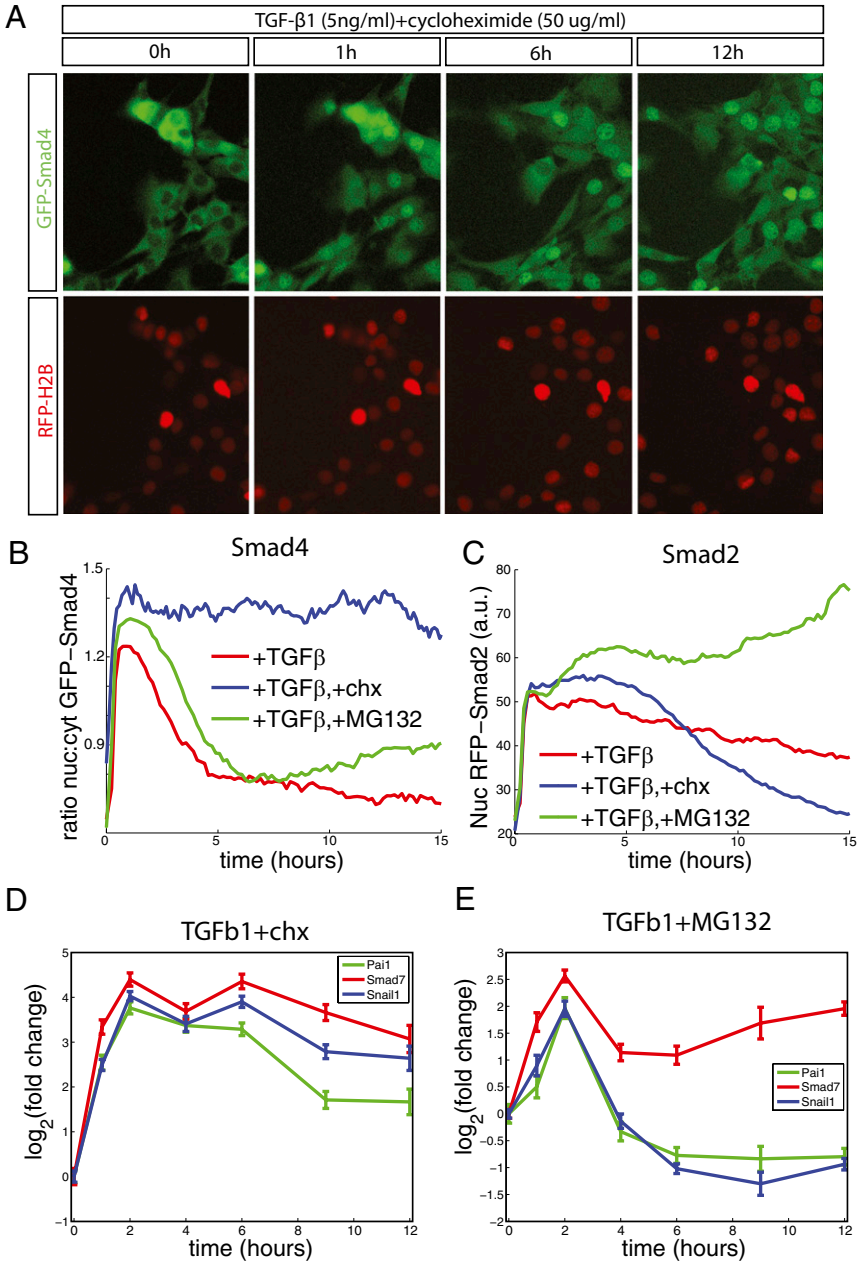

Fig. 4. Smad4 adaptation requires new protein synthesis, and transcriptional dynamics correlate with Smad4 but not Smad2 nuclear accumulation. (*A*) Snapshots from time-lapse imaging of GFP-Smad4 cells treated with TGF-β1 and cycloheximide showing sustained nuclear accumulation of Smad4. (*B*) Quantification of the average ratio of nuclear to cytoplasmic GFP-Smad4 in cells treated with TGF-β1 and either cycloheximide or MG132. Smad4 adaptation requires new protein synthesis but not protein degradation. (*C*) Quantification of nuclear RFP-Smad2 in cells treated with TGF-β1 and either MG132 or cycloheximide. Inhibition of protein synthesis leads to loss of Smad2 from the cell nucleus, whereas inhibition of the proteasome results in continued accumulation of Smad2 in the cell nucleus. (*D* and *E*) Expression of TGF-β target genes by qRT-PCR as a function of duration of treatment in the GFP-Smad4 C2C12 cell line treated with TGF-β1 and either cycloheximide (chx) (*D*) or MG132 (*E*). Inhibiting the proteasome has little effect on dynamics, whereas inhibiting protein synthesis converts the transient response to a sustained one. The increase in Smad7 at long treatment with MG132 may be a homeostatic response to high levels of Smad2 that accumulate after prolonged MG132 treatment (see *C*).

mally in the cell nucleus but began to decline after 6 h and returned to baseline levels after 16 h. Thus, the effects on Smad2 nuclear localization were confined to times relatively late in the response, and both Smad2 and Smad4 show sustained nuclear accumulation in the presence of cycloheximide (Fig. 4 *B* and *C*).

Following individual cells shows a more nuanced picture of the Smad4 response when protein synthesis is inhibited. The initial response of the C2C12 GFP-Smad4 cell line to treatment with TGF-β1 and cycloheximide was uniform, but later the population resolved into high- and low-response groups (Fig. S3 *A* and *B*). Measuring Smad2/3 by immunofluorescence in GFP-Smad4 cells showed a correlation between their levels at both early and late times (Fig. S3 *C* and *D*), but only Smad4 was binary at late times, whereas Smad2/3 was always graded (compare Fig. S3 *B* and *E*). The bimodal distribution of Smad4 and the correlation between Smad2 and 4 at long times suggests that without new protein synthesis cells make a binary decision whether to maintain activation of Smad4 based on the level of activated Smad2/3. A possible mechanism for the binary Smad4 response is presented in the mathematical modeling sections in the *SI Text*.

Transcriptional Dynamics Correlate with Smad4 but Not Smad2 Nuclear Localization. As noted above, inhibiting protein synthesis decreased the duration of Smad2 nuclear accumulation but prolonged Smad4 nuclear accumulation (Fig. 4 *B* and *C*). Thus, the differing effects on Smad2 and Smad4 provided another opportunity to test whether Smad2 or Smad4 controls transcriptional dynamics. Consistent with the retention of Smad4 in the nucleus, target gene expression was prolonged, peaking at 4–6 h after stimulation compared with 2 h without cycloheximide, and target genes still were significantly up-regulated 12 h after stimulation (Fig. 4*D*; compare with Fig. 2*B*). The effects of cycloheximide treatment support our contention that signaling is limited by Smad4 rather than Smad2 nuclear localization, because cycloheximide shortens the duration of Smad2 nuclear localization, lengthens the duration of Smad4 nuclear localization, and lengthens the time for TGF-β–dependent transcription.

Because ubiquitin-dependent degradation has been shown to modulate the extent of Smad2 retention in the nucleus (13), we investigated the effects of proteasome inhibition on Smad2 and Smad4 nuclear accumulation and TGF-β–dependent transcription. Inhibition of the proteasome with MG132 caused the amount of Smad2 in the cell nucleus to increase throughout the period of observation (15 h) (Fig. 4*C*). However, it had very little effect on the dynamics of Smad4 nuclear localization (Fig. 4*B*) and did not prolong the time of expression of TGF-β target genes. (Fig. 4*E*). The dynamics of transcription in cells treated with TGF-β1 and either cycloheximide or MG132 were very similar in the parental and Smad-overexpressing lines (Fig. S3 *F* and *G*). Thus, taken together, the results reported in this section suggest that Smad4 adaptation involves new protein synthesis but not protein degradation and that transcriptional dynamics are affected by perturbations to Smad4 but not Smad2 dynamics.

Either BMP or Activin Signaling Induces Transient Bursts of Nuclear Smad4 in the Early Frog Embryo. To examine TGF-β dynamics in vivo, we turned to the *Xenopus* embryo. During development, TGF-β ligands act as morphogens and play crucial roles in mesoderm induction and dorsal ventral patterning (20–22). We chose to study the animal pole (future ectoderm) of the embryo, because it is patterned by endogenous BMP signaling (23, 24), is responsive to exogenous activin/nodal signaling, and is a convenient tissue for imaging. We began by studying BMP signaling, because BMP signaling is the endogenous signal in this tissue; the animal cap displays no activin/nodal activity.

To study BMP-dependent R-Smad dynamics in the animal cap, we injected mRNA encoding GFP-Smad1 and mCherry-H2B fusion proteins into the embryo at the two-cell stage and dissected the animal pole of the embryo for imaging at the late blastula stage (stage 9). In agreement with a previous study (25), we found that GFP-Smad1 was predominantly nuclear in this tissue. Surprisingly, GFP-Smad1 remained predominantly nuclear even when BMP signaling was inhibited by coexpression of its inhibitors Cerberus, Chordin, or DNAlk3 (Fig. 5*A* and Fig. S4). Strangely, all the BMP inhibitors we tested reduced fluorescence from both GFP-Smad1 and mCherry-H2B; however, the ratio of nuclear to cytoplasmic GFP-Smad1 was reduced only modestly (Fig. 5*B*), suggesting that pathway activity has little effect on the localization of Smad1. Despite the presence of Smad1 in the nucleus, BMP-mediated transcription of an XVent2-luc reporter was repressed strongly by all of the BMP inhibitors tested (Fig. S4*A*). Immunofluorescence for the endogenous protein confirmed nuclear localization of Smad1/5/8 both in untreated animal caps and in the presence of Cerberus (Fig. S4*B*). Thus, nuclear localization of Smad1 is not a reliable indicator of pathway activity in this system, and we turned to assay the status of C-terminally phosphorylated Smad1/5/8. C-terminally phosphorylated Smad1/5/8 was distributed homogeneously throughout animal cap explants (Fig. 5*A*). The staining was specific, because it was inhibited by Cerberus injection (Fig. 5*A*), and injection of the dominant-negative type I BMP receptor Alk3 (DNAlk3) into one cell at the two-cell stage inhibited pSmad1/5/8 specifically in the half-embryo receiving the injection (Fig. S4*C*).

The homogeneous presence of pSmad1 in all cells suggested relatively simple dynamics. To see whether Smad4 localization was similarly homogeneous, we injected mRNAs encoding Venus-Smad4 and mCherry-H2B fusion proteins into both cells of the animal pole of the embryo at the two-cell stage. In blastula-stage animal cap explants, Smad4 showed a striking heterogeneous pattern, strongly accumulated in some nuclei but absent from others (Fig. 5*C*). Heterogeneity was not an imaging artifact, because the nuclear marker mCherry-H2B was clearly detectable in every cell. Time-lapse imaging revealed that the heterogeneity resulted from transient bursts of Smad4 nuclear localization. In nearly every cell, Smad4 entered the nucleus in pulses lasting ~30 min each (Fig. 5*D* and Movie S4). The bursts were uncorrelated spatially with no apparent pattern in timing. Pulses were not periodic, because the time between pulses in the same cell was variable.

Because animal pole cells divide approximately every 30 min during the blastula stage, we examined the time-lapse movies to determine whether cells divided during the pulses of nuclear Smad4. Indeed, cell divisions during the pulses were common; however, examples of pulses both with and without cell divisions could be found readily (Fig. 5*D*). When the cells divided during the pulse, the daughter cells typically showed enhanced nuclear Smad4 after division. Thus, the pulses are not particular to any cell-cycle phase. However, we cannot exclude a role for the cell cycle in the initiation of pulses.

We hypothesized that the bursts of nuclear Smad4 were dependent on the endogenous BMP signaling in the animal pole. Indeed, coinjection of DNAlk3 led to a drastic reduction in the frequency of bursts of nuclear Smad4 (Fig. 6 *A*–*C* and Movie S5), suggesting that BMP signaling is responsible for the pulses of nuclear Smad4. Quantifying nuclear Smad4 as a function of time in single cells, we found that inhibiting BMP signaling led to a large reduction in the number of bursts without affecting the amplitude or duration of the remaining ones (Fig. 6*B* and Fig. S5*A*). The experiments described above showing uniform activation of Smad1/5/8 across the animal cap suggest that the bursting dynamics are limited to Smad4. Quantitatively, we observed no correlation between levels of pSmad1/5/8 and nuclear localization of Smad4 (Fig. S5 *B* and *C*).

Because our mammalian cell-culture studies focused on the TGF-β/activin/nodal branch of the pathway, we sought to address

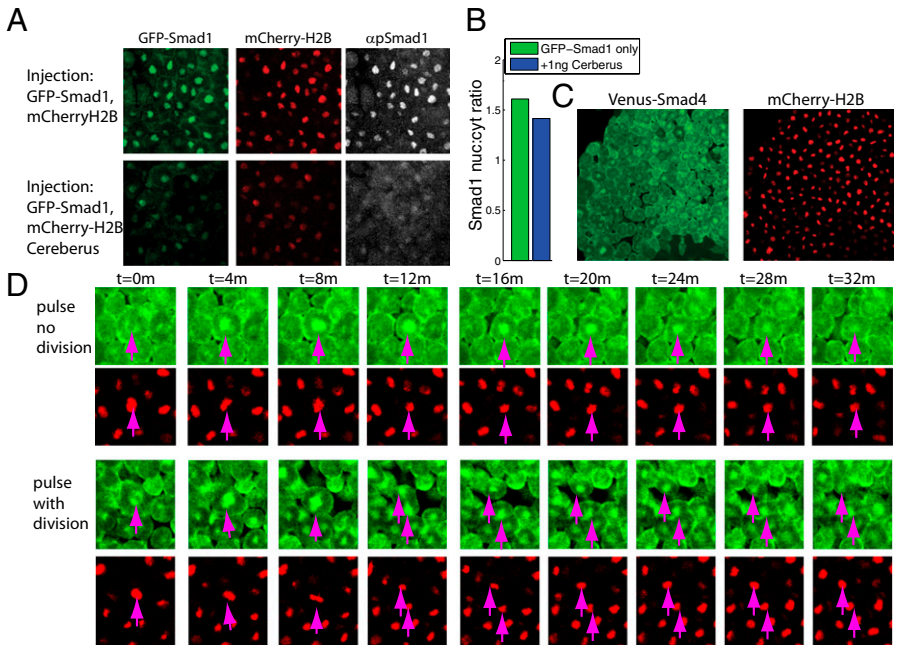

Fig. 5. Smad1 is homogeneously activated, whereas Smad4 is heterogeneous and exhibits brief bursts of nuclear localization in *Xenopus* animal cap explants. (*A*) Smad1 phosphorylation but not Smad1 localization responds to inhibition of BMP signaling. Images are of animal pole tissue from embryos injected at the two-cell stage with 100 pg GFP-Smad1 mRNA and 100 pg mCherry-H2B mRNA in each cell. At stage 9 embryos were fixed and stained by immunofluorescence for pSmad1/5/8. (*B*) Quantification of average nuclear-to-cytoplasmic ratios from the images in *A*. GFP-Smad1 localization does not depend on BMP signaling. (*C*) Smad4 localization is heterogeneous. Images of a stage-9 animal cap explant from an embryo injected at the two-cell stage with 50 pg per cell of Venus-Smad4 mRNA and 100 pg per cell of mCherry-H2B mRNA. (*D*) Zoomed-in image showing the pulses in single cells. (*Upper*) A cell that pulses without dividing. (*Lower*) A cell that divides during the pulse.

whether signaling through this branch could induce similar pulses of activity in *Xenopus* embryos. We prevented the BMP-dependent bursts of nuclear Smad4 by injecting DNAlk3 and then treated the animal cap explants with 10 ng/mL activin. Bursts similar in frequency to those observed in response to endogenous BMP signaling were observed (Fig. 6 *D* and *E* and Movie S6). Immunofluorescent analysis revealed that Smad2/3 accumulated homogeneously in every cell in the animal cap treated with activin (Fig. S5*D*). Similarly, we found that cell dissociation abrogated the BMP-dependent bursts of nuclear Smad4 and that bursts could be restored by treating the dissociated cells with activin (Fig. S5*E*). Taken together, our experiments in the early *Xenopus* embryo show that Smad4, but not the R-Smads, shows repeated pulses of transient activity in response to either BMP or activin signaling and suggest that the temporal duration of signaling is limited by Smad4 as in mammalian cell culture.

Our studies in cell culture showed transient induction of Smad4, whereas those in *Xenopus* embryos showed repeated bursting. To understand the connection between these behaviors, we created a simple mathematical model (*SI Text*, *SI Materials and Methods* and Fig. S6). The result show that transient induction and bursting can coexist readily in the same model and that additional feedback mechanisms could be responsible for creating the bursting dynamics in the *Xenopus* embryo.

Discussion

We have shown that the previously accepted model in which activated, nuclear-localized R-Smads are synonymous with pathway activation need to be refined. Under continuous ligand stimulation, R-Smads remain active, but transcription returns to baseline levels. This basic discrepancy was established using both traditional assays in unmodified cells and live-cell imaging in cells expressing an RFP-Smad2 reporter. In our revision, the R-Smads respond in a uniform, graded manner to the level of agonist. Smad4 enters the nucleus with the R-Smads but then mediates the temporal adaptation of the pathway that terminates transcription. Adaptation requires protein synthesis, but its dynamics do not depend significantly on the agonist level. The heterodimer between the two factors then imposes both digital time control and graded activity on the pathway output.

During the embryonic development, TGF-β ligands act as morphogens with the cell fate outcome dictated not only by the concentration of ligand but also by the timing and duration of stimulation (21, 22). It will be important to reexamine the temporal aspects of TGF-β–mediated fate specification in light of our finding that TGF-β transcription likely is bursting during development. Future work will seek to connect bursts of Smad4 to fate decisions and to determine whether the number of Smad4 bursts plays a role in specifying cell fate. In addition to its role in development, TGF-β is dysregulated in a variety of cancers (26), and the timing of signaling also plays an important role. For example, TGF-β is transiently up-regulated in metastasizing breast cancer cells (27). It seems likely that dysregulation of the timing of signaling will play a role in disease.

Because Smad4 is shared between the two branches of the TGF-β pathway, our model raises further questions about branch interactions (28). If temporal control of the pathway is mediated by Smad4, this control naturally would induce correlations between the timing of TGF-β and BMP-dependent transcription, with the relative amplitudes determined by the activation of branch-specific R-Smads. It will be of interest to determine if adaptation induced by TGF-β will truncate the response to BMP presented a short time later, and conversely. Of equal interest is the response to temporal pulses of agonist. Is there a refractory period defined by the adaptation?

Our model postulates that the duration of Smad4 nuclear localization is independent of that for R-Smads and coincides with the timing of transcription. Although there is abundant evidence

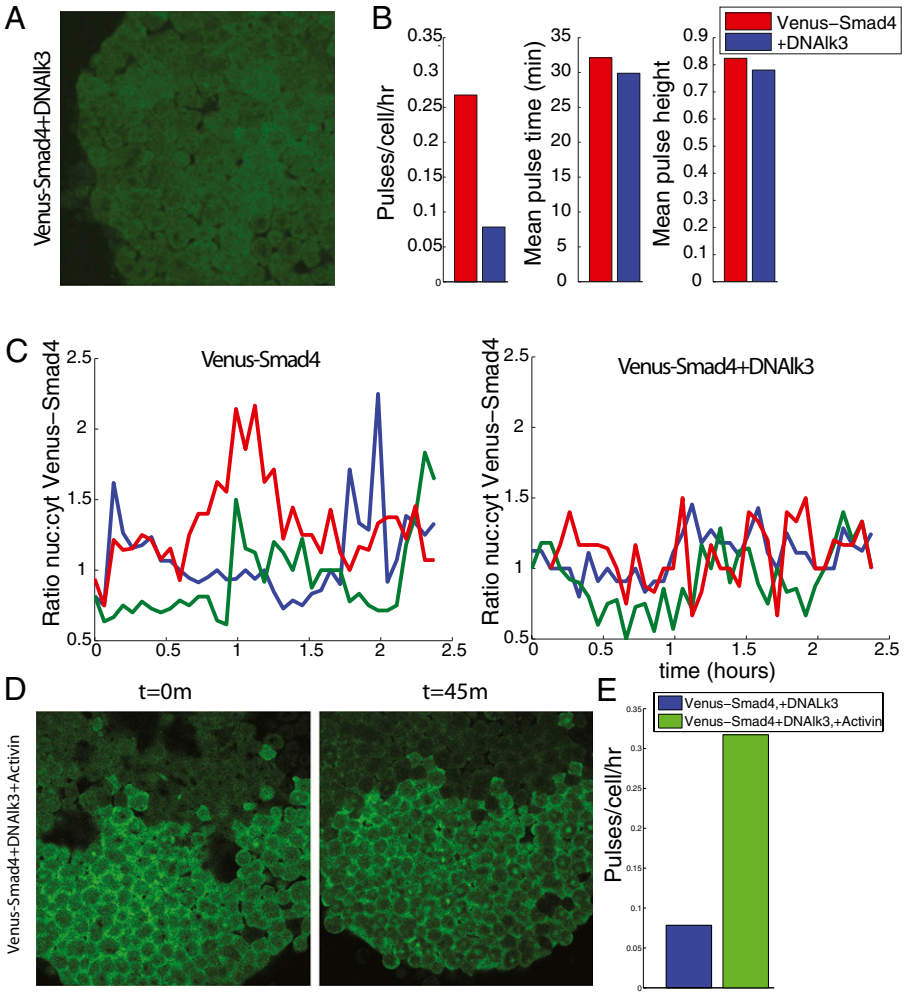

Fig. 6. Pulses of nuclear Smad4 can be induced by either BMP or activin/nodal signaling in *Xenopus* animal cap explants. (*A*) Pulses are dependent on endogenous BMP signaling. Image of a stage-9 animal cap explant in which 50 pg Venus Smad4 and 100 pg mCherry-H2B mRNA were coinjected with 1 ng of the BMP inhibitor DNAlk3 mRNA. The animal cap explant shown is from a sibling embryo of the one used to make the explants shown in Fig. 5 *C* and *D* with injections and imaging performed at the same times. (*B*) Quantification of number of pulses and pulse height and duration. (*C*) Quantification of single-cell traces from the time-lapse movies. (*D*) Response of Smad4 to activin treatment. Embryos were injected in the animal pole with Venus-Smad4, mCherry-H2B, and DNAlk3 mRNAs to inhibit BMP signaling. Animal cap explants were dissected at stage 9 and treated with activin. Pictures are shown before (*Left*) or 45 m after (*Right*) activin treatment. (*E*) Quantification of number of bursts in animal cap explants injected with Venus-Smad4 and DNAlk3 and either left untreated or treated with activin (10 ng/mL).

that nuclear-localized, activated R-Smads are necessary for transcription, it is worth reviewing the experiments leading to the previous model that temporal control is regulated primarily through the R-Smads. Because Smad4 is not phosphorylated by the receptors or inactivated by linker phosphorylation, it appeared as the passive cofactor to the R-Smads. The nuclear import of Smad4 in response to agonist requires the R-Smads (8), and inhibiting the pathway at the receptor level with SB431542 or Noggin causes export of both R-Smads and Smad4 (17). Also the timing of nuclear Smad4 and transcription of pathway targets was examined in several experiments (17, 29) but always in the presence of cycloheximide (*SI Text*) and thus do not contradict our conclusions. In both *Xenopus* animal caps and sparsely plated HaCaT cells we found Smad4 localization is intermittent but clearly is signaling dependent. Thus, population assays for nuclear Smad4 (29) should show that it varies with the activated nuclear R-Smads. Discrepancies among other experiments (*SI Text*) involving the duration of the transcriptional response in HaCaT cells may be explained by cell density, because in dense cultures Smad4 localization follows the same dynamics as in C2C12 cells (Fig. S2).

Experiments with transgenic mice challenge the notion that Smad4 localization is mechanistically responsible for the termination of transcription. Mice homozygous for a constitutively nuclear Smad4 appear normal (30). Presumably the duration of TGF-β signaling must be close to that in wild-type embryos to permit normal development. Thus, we favor the model that Smad4 nuclear export is downstream of pathway inactivation but is not causal to termination of transcription. Indeed the fractional changes in nuclear Smad4 that we observe would be inadequate to explain the differences in transcriptional output in a simple physical–chemical model of Smad heterodimer formation. Multiple biochemical events may be collectively responsible for the adaptation we found in the transcriptional response of the TGF-β pathway to a step stimulus. One possibility is SnoN repression of Smad2/3 transcriptional targets (31). This factor is degraded by TGF-β signaling but also is a transcriptional target of TGF-β, thus explaining the effect we see with cycloheximide. Second, Smad4 monoubiquitination disrupts the complex with

R-Smads and inhibits pathway activity (32, 33). Similarly, Smad4 sumoylation also can inhibit the pathway (34, 35). The fact that the adaption is reflected only in Smad4 excludes negative feedback mechanisms, such as induction of the inhibitory Smad7 or degradation of activated R-Smads, that primarily target R-Smads or receptors.

There is a large literature on time-dependent signaling (reviewed in ref. 36) motivated by the realization that the same pathway can link different stimuli to distinct transcriptional targets. A logical source for the information governing specificity is the time course of the signal or the temporal activity of pathway intermediates. A system that merits comparison with the present work is NFκB (2, 3). The single-cell data (3) following nuclear localization of NFκB in response to a step in TNF-α show a largely digital and adaptive response (but see ref. 37). The intensity of the step defines the fraction of cells that respond, and the nuclear-localized NFκB returns to near base line in 90 min. In contrast, although we observe adaptation in response to ligand stimulation, we do not find a binary response for intermediate ligand levels; rather, all cells respond. An earlier study on NFκB dynamics observed less adaptation and more pronounced oscillations (38), and it may be that the microfluidic chambers in the more recent study allow cell-secreted factors or ligand depletion to modulate the response (3).

Signaling pathways commonly exhibit multiple levels of negative feedback operating on the receptors, factor localization by posttranscriptional modifications, and transcription of inhibitory factors. All potentially can generate bursts of activity, as in the p53 system (4, 39). In analogy to our observations in *Xenopus* experiments, where the bursts changed in number but not shape in response to pathway inhibition, the p53 bursts are present in normally cycling cells and become more frequent with DNA damage (4). Adaptation is another consequence of pathway negative feedback and can depend on secondary interactions among the principal pathway components. A notable example is in PC-12 cells, where the Erk response is adaptive in response to EGF but sustained in response to NGF (40).

As our experiments in mammalian culture cells and *Xenopus* embryos reveal, the behavior of Smad4 can be either adaptive or pulsatile, depending on the context. Our mathematical modeling suggests that these behaviors are closely connected and that the same model can encompass both. Additional feedbacks or external inputs such as those from cell-to-cell contacts, cross-talk with other pathways, or the cell cycle could serve to generate pulsing or oscillatory behaviors from a core adaptive circuit. Distinguishing these possibilities will require further dissection of the mechanisms controlling temporal control of Smad4 nuclear localization and transcription.

Materials and Methods

Constructs. All constructs for cell-culture studies were cloned into ePiggyBac vectors, and all constructs for *Xenopus* experiments were cloned in the pCS2+ vector. Details can be found in *SI Materials and Methods*.

Cell Culture, Transfections, and Selection of Stable Lines. Both C2C12 and HaCaT cells were maintained in DMEM containing 10% (vol/vol) FBS. All transfections were performed with Lipofectamine 2000 (Invitrogen) according to the manufacturer's instructions. Following the transfections, cells were selected with blasticidin (10 μg/mL), puromycin (4 μg/mL), or Zeocin (500 μg/mL). Clonal lines were established by plating as single cells and selecting clones manually.

Reagents. Cycloheximide was purchased from Sigma-Aldrich and was used at a concentration of 50 μg/mL to inhibit protein synthesis (29, 41). MG132 was purchased from Sigma-Aldrich and used at a concentration of 10 μM to inhibit proteasomal degradation (42). SB431542 was purchased from Tocris Bioscience and used at a concentration of 10 μM to inhibit Smad2/3 phosphorylation (12). TGF-β1 and activin A were purchased from R&D Systems and used at the concentrations indicated in the text.

***Xenopus* Embryo Manipulation.** Eggs were collected, fertilized in vitro, dejellied, and injected with mRNA using standard techniques (*SI Materials and Methods*). For imaging of animal caps, animal caps were dissected at stage 9 and grown on fibronectin-coated glass in a low-calcium medium that does not dissociate cells but prevents rounding of animal caps, which occurs rapidly in normal explant medium.

Live Cell Imaging and Image Analysis. C2C12 and HaCaT cells were plated in glass-bottomed dishes (MatTek) at least 1 d before imaging. Imaging was performed in L15 medium containing 10% (vol/vol) FBS using an IX71 Olympus inverted microscope with a 20×, 0.75 Na lens. *Xenopus* animal caps were placed on glass-bottomed dishes that had been coated with fibronectin (20 μg/mL) (Sigma) and imaged using an inverted Zeiss confocal microscope (LSM 510) with a 20×, 0.7 Na lens and collecting a Z stack containing four to six slices every 3–5 min. Image analysis was performed with custom software written in MATLAB as described in *SI Materials and Methods*.

Immunofluorescence. Immunofluorescence on culture cells was performed using standard techniques. Immunofluorescence in *Xenopus* animal caps was performed according to the procedure described by Larabell et al. (43). Details and antibodies can be found in *SI Materials and Methods*.

Western Blotting and qRT-PCR. Western blotting and qRT-PCR were performed using standard methods. Antibodies and primers are listed in *SI Materials and Methods*.

Luciferase Assays. At the two- or four-cell stage, 15 pg of XVent-luc reporter plasmid was injected into each cell. At stage 11, four embryos were lysed together in 50 μL of passive lysis buffer (Promega), and the luciferase assay was performed using the Promega luciferase assay system according to the manufacturer's instructions. CAGA12 and 3TP experiments in C2C12 cells were performed using the dual luciferase assay kit (Promega). Details can be found in *SI Materials and Methods*.

ACKNOWLEDGMENTS. We thank Darym Alden and Sasa Jereb for technical assistance, Paul Francois for a critical reading of the manuscript, and members of the A.H.B. and E.D.S. laboratories for helpful discussions. We thank J. Gurdon for providing the GFP-Smad1 plasmid. Funding supporting this work was provided by the Emerald Foundation, The Rockefeller University, NYSTEM, National Institutes of Health Grant R01 HD32105 (to A.H.B.), and National Science Foundation Grant PHY-0954398 (to E.D.S.).

1. Brivanlou AH, Darnell JE, Jr. (2002) Signal transduction and the control of gene expression. *Science* 295:813–818.
2. Hoffmann A, Levchenko A, Scott ML, Baltimore D (2002) The IkappaB-NF-kappaB signaling module: Temporal control and selective gene activation. *Science* 298: 1241–1245.
3. Tay S, et al. (2010) Single-cell NF-kappaB dynamics reveal digital activation and analogue information processing. *Nature* 466:267–271.
4. Loewer A, Batchelor E, Gaglia G, Lahav G (2010) Basal dynamics of p53 reveal transcriptionally attenuated pulses in cycling cells. *Cell* 142:89–100.
5. Wu MY, Hill CS; MY (2009) Tgf-β superfamily signaling in embryonic development and homeostasis. *Dev Cell* 16:329–343.
6. Massagué J, Seoane J, Wotton D (2005) Smad transcription factors. *Genes Dev* 19: 2783–2810.
7. Schmierer B, Hill CS (2005) Kinetic analysis of Smad nucleocytoplasmic shuttling reveals a mechanism for transforming growth factor beta-dependent nuclear accumulation of Smads. *Mol Cell Biol* 25:9845–9858.
8. Liu F, Pouponnot C, Massagué J (1997) Dual role of the Smad4/DPC4 tumor suppressor in TGFbeta-inducible transcriptional complexes. *Genes Dev* 11:3157–3167.
9. Fuentealba LC, et al. (2007) Integrating patterning signals: Wnt/GSK3 regulates the duration of the BMP/Smad1 signal. *Cell* 131:980–993.
10. Gao S, et al. (2009) Ubiquitin ligase Nedd4L targets activated Smad2/3 to limit TGF-beta signaling. *Mol Cell* 36:457–468.
11. Lacoste A, Berenshteyn F, Brivanlou AH (2009) An efficient and reversible transposable system for gene delivery and lineage-specific differentiation in human embryonic stem cells. *Cell Stem Cell* 5:332–342.
12. Inman GJ, et al. (2002) SB-431542 is a potent and specific inhibitor of transforming growth factor-beta superfamily type I activin receptor-like kinase (ALK) receptors ALK4, ALK5, and ALK7. *Mol Pharmacol* 62:65–74.
13. Lo RS, Massagué J (1999) Ubiquitin-dependent degradation of TGF-beta-activated smad2. *Nat Cell Biol* 1:472–478.
14. Sapkota G, Alarcón C, Spagnoli FM, Brivanlou AH, Massagué J (2007) Balancing BMP signaling through integrated inputs into the Smad1 linker. *Mol Cell* 25:441–454.

15. Dennler S, et al. (1998) Direct binding of Smad3 and Smad4 to critical TGF beta-inducible elements in the promoter of human plasminogen activator inhibitor-type 1 gene. *EMBO J* 17:3091–3100.
16. Wrana JL, et al. (1992) TGF beta signals through a heteromeric protein kinase receptor complex. *Cell* 71:1003–1014.
17. Inman GJ, Nicolás FJ, Hill CS (2002) Nucleocytoplasmic shuttling of Smads 2, 3, and 4 permits sensing of TGF-beta receptor activity. *Mol Cell* 10:283–294.
18. Varelas X, et al. (2010) The Crumbs complex couples cell density sensing to Hippo-dependent control of the TGF-β-SMAD pathway. *Dev Cell* 19:831–844.
19. Watanabe M, Masuyama N, Fukuda M, Nishida E (2000) Regulation of intracellular dynamics of Smad4 by its leucine-rich nuclear export signal. *EMBO Rep* 1:176–182.
20. De Robertis EM, Kuroda H (2004) Dorsal-ventral patterning and neural induction in *Xenopus* embryos. *Annu Rev Cell Dev Biol* 20:285–308.
21. Green JB, New HV, Smith JC (1992) Responses of embryonic *Xenopus* cells to activin and FGF are separated by multiple dose thresholds and correspond to distinct axes of the mesoderm. *Cell* 71:731–739.
22. Wilson PA, Lagna G, Suzuki A, Hemmati-Brivanlou A (1997) Concentration-dependent patterning of the *Xenopus* ectoderm by BMP4 and its signal transducer Smad1. *Development* 124:3177–3184.
23. Faure S, Lee MA, Keller T, ten Dijke P, Whitman M (2000) Endogenous patterns of TGFbeta superfamily signaling during early *Xenopus* development. *Development* 127: 2917–2931.
24. Schohl A, Fagotto F (2002) Beta-catenin, MAPK and Smad signaling during early *Xenopus* development. *Development* 129:37–52.
25. Simeoni I, Gurdon JB (2007) Interpretation of BMP signaling in early *Xenopus* development. *Dev Biol* 308:82–92.
26. Padua D, Massagué J (2009) Roles of TGFbeta in metastasis. *Cell Res* 19:89–102.
27. Giampieri S, et al. (2009) Localized and reversible TGFbeta signalling switches breast cancer cells from cohesive to single cell motility. *Nat Cell Biol* 11:1287–1296.
28. Candia AF, et al. (1997) Cellular interpretation of multiple TGF-beta signals: Intracellular antagonism between activin/BVg1 and BMP-2/4 signaling mediated by Smads. *Development* 124:4467–4480.
29. Pierreux CE, Nicolás FJ, Hill CS (2000) Transforming growth factor beta-independent shuttling of Smad4 between the cytoplasm and nucleus. *Mol Cell Biol* 20:9041–9054.
30. Biondi CA, et al. (2007) Mice develop normally in the absence of Smad4 nucleocytoplasmic shuttling. *Biochem J* 404:235–245.
31. Stroschein SL, Wang W, Zhou S, Zhou Q, Luo K (1999) Negative feedback regulation of TGF-beta signaling by the SnoN oncoprotein. *Science* 286:771–774.
32. Dupont S, et al. (2009) FAM/USP9x, a deubiquitinating enzyme essential for TGFbeta signaling, controls Smad4 monoubiquitination. *Cell* 136:123–135.
33. Agricola E, Randall RA, Gaarenstroom T, Dupont S, Hill CS (2011) Recruitment of TIF1γ to chromatin via its PHD finger-bromodomain activates its ubiquitin ligase and transcriptional repressor activities. *Mol Cell* 43:85–96.
34. Lee PSW, Chang C, Liu D, Derynck R (2003) Sumoylation of Smad4, the common Smad mediator of transforming growth factor-beta family signaling. *J Biol Chem* 278: 27853–27863.
35. Long J, Wang G, He D, Liu F (2004) Repression of Smad4 transcriptional activity by SUMO modification. *Biochem J* 379:23–29.
36. Behar M, Hoffmann A (2010) Understanding the temporal codes of intra-cellular signals. *Curr Opin Genet Dev* 20:684–693.
37. Cheong R, Rhee A, Wang CJ, Nemenman I, Levchenko A (2011) Information transduction capacity of noisy biochemical signaling networks. *Science* 334:354–358.
38. Nelson DE, et al. (2004) Oscillations in NF-kappaB signaling control the dynamics of gene expression. *Science* 306:704–708.
39. Batchelor E, Mock CS, Bhan I, Loewer A, Lahav G (2008) Recurrent initiation: A mechanism for triggering p53 pulses in response to DNA damage. *Mol Cell* 30: 277–289.
40. Santos SDM, Verveer PJ, Bastiaens PIH (2007) Growth factor-induced MAPK network topology shapes Erk response determining PC-12 cell fate. *Nat Cell Biol* 9:324–330.
41. Xiao Z, Latek R, Lodish HF (2003) An extended bipartite nuclear localization signal in Smad4 is required for its nuclear import and transcriptional activity. *Oncogene* 22: 1057–1069.
42. Alarcón C, et al. (2009) Nuclear CDKs drive Smad transcriptional activation and turnover in BMP and TGF-beta pathways. *Cell* 139:757–769.
43. Larabell CA, et al. (1997) Establishment of the dorso-ventral axis in *Xenopus* embryos is presaged by early asymmetries in beta-catenin that are modulated by the Wnt signaling pathway. *J Cell Biol* 136:1123–1136.

Supporting Information

Warmflash et al. 10.1073/pnas.1207607109

SI Text

Mathematical Modeling. Our studies in cell culture showed transient induction of Smad4, whereas studies in *Xenopus* embryos showed repeated bursting. To understand the connection between these behaviors, we created a simple mathematical model (Fig. S6*A*). In this model, ligand activates the R-Smad, and activated R-Smad causes Smad4 to move the nucleus. Based on our data showing that Smad4 is exported from the nucleus in a manner dependent on new protein synthesis, we postulate that ligand addition causes the synthesis of another component (denoted "X") that mediates Smad4 export from the nucleus. In agreement with our experiments, this model shows adaptive behavior, pulsing once in response to a step increase in ligand concentration and then returning to baseline levels (Fig. S6*B*). The explanation for the adaptation is that the factors mediating both the import and export of Smad4 from the nucleus [receptor-regulated Smads (R-Smads) and X, respectively] are dependent on the ligand concentration but have different kinetics. R-Smad is activated more rapidly than X because R-Smads are activated through phosphorylation, whereas X is newly synthesized in response to TGF-β. The difference in kinetics causes an initial increase in the amount of active R-Smad relative to X, leading to nuclear import of Smad4; at steady state, however, both R-Smad and X are activated in proportion to the ligand levels, so the effects on the activation of Smad4 cancel out.

We hypothesized that additional feedbacks may be present in the *Xenopus* embryo and may cause the repeated pulses. To test whether this scenario is plausible in the model, we added feedback onto the production of the ligand from active Smad4. Indeed, simple linear feedback caused the model to switch from adaptive to oscillatory behavior (Fig. S6*C*). The same model was used to describe adaptive temperature compensation in circadian oscillations (1). This connection between adaptive and oscillatory behavior is likely to be general, because the addition of feedback to a minimal model of an adaptive system also resulted in oscillatory behavior.

Finally, we note that the model provides an explanation for the binary nuclear accumulation of Smad4 when cells were treated with TGF-β1 and cycloheximide (Fig. 4*A* and Fig. S3). The steady-state levels of nuclear Smad4 depend on the ratio of active R-Smad to X. As is well known, systems in which a substrate is activated and inactivated by opposing enzymes can generate ultrasensitive behavior: If the activity of the activating enzyme exceeds that of the inactivating enzyme, the substrate will be primarily in the active state, whereas the opposite configuration results in the substrate existing primarily in the inactive state. Thus, there is an ultrasensitive transition from primarily active to primarily inactive at the point where the activities of the two enzymes balance (2). When cells are treated with TGF-β1 and cycloheximide, the level of active Smad2 increases, causing activation of Smad4; however, in the presence of cycloheximide, nuclear Smad2 levels start to decline after 6 h of continuous stimulation (Fig. 4*C*). In the model, when the level of R-Smad activity falls below the basal level of X activity, there is a sharp transition from active to inactive Smad4 (Fig. S6*D*). Because the levels of active Smad2 or X will differ from cell to cell, different cells will switch off at different times, resulting in a bistable distribution across the population. Consistent with this hypothesis, localization of Smad4 to the nucleus correlates with increased nuclear Smad2 (Fig. S3).

Prior Literature on the Termination of TGF-β Signaling Under Continuous Pathway Stimulation. The activation of the R-Smads by their cognate receptors is necessary for a transcriptional response to TGF-β signaling. The regulation of the phosphorylation status of the R-Smads and the ultimate fate of activated R-Smads is an intensely studied subject. As such, it is natural to assume that signaling will persist as long as activated R-Smads remain in the nucleus. Further, it was shown that nuclear import of Smad4 in response to agonists requires the R-Smads (3), and thus it was assumed that the localization of Smad4 is slaved to that of the R-Smads. Our results contradict the suppositions that (*i*) Smad agonist mediated transcription persists as long as R-Smads are nuclear, and (*ii*) nuclear localization of Smad4 follows the R-Smads. We have screened prior literature for any contradictory data and find none. Our paper argues that the nuclear localization of the R-Smads and Smad4 follow different dynamics, although under a number of conditions their dynamics would appear the same:

i) In two widely studied contexts, the *Xenopus* embryo and HaCaT cells, bursts of nuclear Smad4 are asynchronous across the cell population. As such, even though the dynamics of R-Smads and Smad4 may differ at the level of individual cells, the bulk dynamics as measured by Western blotting applied to lysates from nuclear extracts would be similar.

ii) Treating cells with cycloheximide removes the feedback responsible for shutdown of the pathway and restores correlation between the R-Smads and Smad4 even at the level of individual cells. Many experiments are done in the presence of cycloheximide to avoid secondary effects.

iii) Shutdown of the pathway at the level of the R-Smads (e.g., by using the receptor inhibitor SB431542 or Noggin), causes nuclear export of both R-Smads and Smad4, and thus the dynamics of pathway shutoff in the presence of these inhibitors will be similar for R-Smads and Smad4.

As a result, although our study alters the standard view of how the dynamics of the pathway are regulated, we do not find any contradictory data in the literature. Among the papers we consulted are the studies noted below (4–13).

Study by Pierreux et al. The paper by Pierreux et al. (4) largely addresses the function of various alternative splice variants of Smad4; however, in their figure 7 it is shown, using Western blotting on nuclear extracts, that Smad2 and Smad4 have the same kinetics exiting the nucleus after ∼6 h in HaCaT cells subjected to continuous stimulation. Because the cells were pretreated with cycloheximide, this result is to be expected according to item *ii*) above.

Study by Inman et al. Using SB431542 to inhibit of TGF-β type I receptor kinase function, Inman et al. (5) show continual recycling of C-terminally phosphorylated Smad2, thus suggesting that the transcriptional response is continuous as long as phosphorylated Smad 2 (pSmad2) is present. Cycloheximide treatment results in more rapid decay of pSmad2, as we find. New transcription as measured by CAGA12-luciferase or DE-luciferase constructs ceases after 4 h (figure 1 in ref. 5). Immunofluorescence against Smad2/3 and Smad4 shows fairly coherent expression of both markers through 4 h (figure 3 in ref. 5), but the cells were pretreated with cycloheximide, so there is no contradiction with our results.

Study by Biondi et al. Mice homozygous for a constitutively nuclear Smad4 appear normal (6). Presumably the duration of TGF-β signaling must be close to that in WT to permit normal de-

velopment. Thus, we favor the model that Smad4 nuclear export is downstream of pathway inactivation but is not causal. Indeed the fractional changes in nuclear Smad4 that we observe would be inadequate to explain the differences in transcriptional output in a simple physical–chemical model of Smad heterodimer formation.

Transcriptional response in HaCaT cells. Under continuous stimulation in sparse cultures, we observe spatially incoherent but long-term nuclear Smad4, and one would expect that transcription is similarly extended compared with C2C12 cells (Fig. 2), as is shown in figure 1 E–G of Dai et al. (7) and in figure 7C of Gao et al. (8). Note that these results for qPCR suggest that TGF-β–dependent transcription persists longer than suggested by the luciferase assays done by Inman et al. (5) and described above. The difference between experiments may be explained by differences in culture density. Our results show that in dense cultures Smad4 relocalizes to the cytoplasm after ∼4 h, as is consistent with the results of Inman et al., but in sparse cultures Smad4 remained heterogeneously nuclear for a prolonged period after stimulation, consistent with long-term transcription following TGF-β stimulation (Fig. S2).

Long-lived activation of Smad2/3. Our study suggests that Smad2/3 activation peaks at 1–2 h following ligand stimulation but the decay thereafter is relatively modest, and overall Smad2/3 remains nuclear and phosphorylated as long as ligand is present. Several studies have suggested mechanisms by which signaling is inhibited at the level of Smad2/3 through degradation (8, 9), nuclear export (7), or dephosphorylation (9). However, none of these studies examined the time required for pSmad2/3 to return to its baseline level under continuous stimulation. In contrast, other studies have argued for long-lived activation of Smad2/3 (10). Overall, all studies are consistent with the idea that these factors targeting Smad2/3 modulate the intensity of the response but do not return signaling to its baseline level.

Localization of R-Smads in* Xenopus *animal cap explants. We show in the main text that Smad1/5/8 are phosphorylated uniformly in the animal cap in a bone morphogenic protein (BMP) signaling-dependent manner. Surprisingly, although inhibiting the BMP pathway resulted in a striking decrease in pSmad1/5/8 (Fig. 5*A*) and BMP-dependent transcription (Fig. S4), it had little effect on the localization of either GFP-Smad1 or endogenous Smad1/5/8 as measured by immunofluorescence (Fig. 5*A* and Fig. S4). We obtained similar results whether the BMP pathway was inhibited by injection of mRNA encoding DNAlk3 or by extracellular inhibitors such as Chordin and Noggin. This outcome is in agreement with the results in Simeoni and Gurdon (11) who found that GFP-Smad1 localized to the nucleus even in dissociated cells.

We also attempted to monitor the dynamics of Smad2 using a published GFP-xSmad2 fusion construct (12); however, in our hands, in animal cap explants GFP-xSmad2 showed considerably more nuclear localization than endogenous Smad2 in the absence of signal, and there was little measurable nuclear accumulation with the addition of activin. In contrast, endogenous Smad2/3, as measured by immunofluorescence, showed little nuclear accumulation in the absence of applied ligands and dramatic relocalization to the nucleus upon ligand addition (Fig. S5). We do not know how to explain this discrepancy between our results and those obtained by other investigators (12, 13).

SI Materials and Methods

Constructs. All constructs for cell-culture studies were cloned in ePiggyBac vectors (14) with a CAG promoter and blasticidin, puromycin, or Zeocin resistance (denoted ePB-B-CAG, ePB-P-CAG, and ePB-Z-CAG, respectively). For GFP-Smad4 and RFP-Smad2, we used PCR cloning to clone the fluorescent protein into the BamHI site of ePB-B-CAG using a BglII site at the 5′ end of the fluorescent protein and a BamHI site at the 3′ end. We then used PCR cloning to insert hSmad4 into ePB-B-CAG-GFP with BamHI-NotI and mSmad2 into ePB-B-CAG-RFP with HindIII-NotI. For unlabeled Smad2, we cloned the same HindIII-NotI fragment into ePB-P-CAG. For the GFP-nuclear localization signal (NLS) we used the same strategy to clone GFP into the BamHI site of ePB-P-CAG. We then annealed synthetic oligos encoding three repeats of the NLS and inserted them into BamHI-NotI. For RFP-H2B, the HindIII-NotI TagRFP-H2B fragment was cut from pTagRFP-H2B (Evrogen) and ligated into ePB-Z-CAG.

Constructs for *Xenopus* embryos were cloned into the pCS2+ vector. Venus fluorescent protein and hSmad4 were cloned by PCR into the EcoRI-XhoI and XhoI-XbaI sites to make pCS2+Venus-Smad4. mCherry fluorescent protein, and xH2B was cloned into the BamHI-XhoI and XhoI-XbaI sites to create pCS2+mCherry-xH2B. mRNA was synthesized using the SP6 mMessage mMachine kit (Ambion) according to the manufacturer's instructions. The XVent2-luc (15), pCS107-GFP-Smad1 (11), pCS2+Cerberus, and pSP64T-DNAlk3 (16) constructs have been described previously.

Cell Culture, Transfections, and Selection of Stable Lines. Both C2C12 and HaCaT cells were maintained in DMEM containing 10% FBS. All transfections were performed with Lipofectamine 2000 (Invitrogen) according to the manufacturer's instructions. To make the RFP-Smad2 cell line, we transfected C2C12 cells with ePB-B-RFP-Smad2 and ePB-P-GFP-NLS together with a plasmid encoding the ePB transposase (14). Cells were selected with 10 μg/mL blasticidin and 4 μg/mL puromycin. To make the GFP-Smad4 cell line, we first transfected ePB-B-CAG-GFP-Smad4, ePB-P-CAG-Smad2, and the ePB transposase and selected with blasticidin and puromycin. We then transfected the resulting cells with ePB-Z-CAG-RFP-H2B and selected with blasticidin, puromycin, and Zeocin (500 μg/mL). In both cases, we isolated clonal lines by plating cells sparsely and selecting clones manually. In each case, we screened six clones and chose for our studies the lines with the lowest overexpression of the Smad proteins with detectable fluorescence in both the GFP and RFP channels and a strong response to TGF-β1 stimulation. Following selection, cells were maintained in medium containing the selecting antibiotics at half of the concentration used for selection.

Reagents. Cycloheximide was purchased from Sigma-Aldrich and was used at a concentration of 50 μg/mL to inhibit protein synthesis (4, 5). MG132 was purchased from Sigma-Aldrich and was used at a concentration of 10 μM to inhibit proteasomal degradation (17). SB431542 was purchased from Tocris Bioscience and was used at a concentration of 10 μM to inhibit Smad2/3 phosphorylation (18). TGF-β1 and activin A were purchased from R&D Systems and used at the concentrations indicated in the main text.

***Xenopus* Embryo Manipulation.** Eggs were collected, fertilized in vitro, dejellied before the first cell division in 3.5% cysteine, and injected with mRNA at the two-cell stage. Injections were performed in 3.5% Ficoll, 0.5× Marc's modified ringer (MMR), and embryos were grown in this solution until stage 8–9. For imaging of animal caps, animal caps were dissected at stage 9 and grown on fibronectin-coated glass in a low-calcium medium [1:1 mixture of calcium- and magnesium-free medium (CMFM) and low-calcium and -magnesium Ringer containing 0.1% BSA; (19)]. This medium does not dissociate cells but prevents the rounding and closing of animal caps that occurs rapidly in normal explant media. For cell dissociation, animal caps were dissected and placed in CMFM containing 0.1% BSA for 15 min. Then the pigmented outer layer of cells was peeled off, and the dissociated inner cells were collected and seeded on fibronectin-coated glass.

Live-Cell Imaging. For imaging of C2C12 and HaCaT cells, we plated cells in glass-bottomed dishes (MatTek) at least 1 d before imaging. Immediately before imaging, we switched the cell medium to L15 medium containing 10% FBS, which is substantially less fluorescent than DMEM. We collected images every 5–8 min using an IX71 Olympus inverted microscope with a 20×, 0.75 Na lens. For imaging of *Xenopus* animal caps, 30 min before imaging, animal caps were placed on glass-bottomed dishes that had been coated with fibronectin (20 μg/mL) (Sigma) for 2 h. We used an inverted Zeiss confocal microscope (LSM 510) with a 20×, 0.7 Na lens and collected a Z stack containing four to six slices every 3–5 min. To avoid cross-talk between the yellow and red channels, we imaged Venus-Smad4 using settings for GFP (488 nm excitation; 500–530 nm emission).

Image Quantification. Image analysis was performed using custom software written in MATLAB. We used the nuclear marker images to identify nuclei using an algorithm that identifies local maxima and then detects the edges of each nucleus by examining the contour height of the maximum intensity gradient. We identified the cytoplasm of each cell either by applying a method similar to that used for the Smad fluorescence image; when this approach was not possible (e.g., Smad2 in cells stimulated with TGF-β1 is almost exclusively nuclear), we used a narrow donut around the nucleus with radius chosen so that it almost certainly was contained in the cell. Smad fluorescence was computed by examining the average values of nuclear and cytoplasmic fluorescence in the masks defined by this procedure. For the Z stacks from *Xenopus* experiments, we made a maximum intensity projection of the nuclear marker images and used the resulting image to identify nuclei. Then, for each cell, we performed the analysis of Smad fluorescence in the *z*-plane in which the nuclear marker was most intense. After identification of nuclei, cells were tracked through time using the algorithm described in Sbalzarini and Koumoutsakos (20). Single-cell trajectories presented in the paper were examined manually to avoid errors from the automatic analysis.

For identification of Smad4 bursts in the *Xenopus* experiments, we first fit the raw fluorescence traces to a smoothing spline and then found the maxima and minima of the smoothed trajectory. We then took the raw data from the time points between consecutive minima and scaled the data to fall between 0 and 1 according to the formula $(x_i - \min(x))/(\max(x) - \min(x))$. We then considered the "burst" to be the connected region containing the maxima so that the rescaled value of the points in the region was greater than 0.3 and used this definition of the burst to compute its amplitude and duration.

Immunofluorescence. Cells were plated in glass-bottomed dishes at least 1 d before the experiment. After stimulation, cells were rinsed once with PBS, fixed with 4% paraformaldehyde for 20 min, rinsed twice with PBS, blocked for 30 min with 3% donkey serum and 0.1% Triton X-100 in PBS, and then were incubated overnight at 4 °C with primary antibodies diluted in blocking buffer. Antibodies were αSmad2/3 (dilution 1:100) (610842; BD Transduction Labs) and αSmad4 (dilution 1:100) (B8; Santa Cruz). Cells then were washed three times with PBS, 0.1% Tween 20 for 30 min each wash, incubated for 30 min with secondary antibodies (Alexa 488 or Alexa 647; dilution 1:400) and Sytox (dilution 1:25,000) diluted in blocking buffer, and washed twice more with PBS, 0.1% Tween 20 for 30 min each wash.

Immunofluorescence in *Xenopus* animal caps was performed according to the procedure described in Larabell et al. (21). Briefly, whole embryos were fixed either overnight at 4 °C or for 2 h at room temperature in 4% paraformaldehyde, 0.1% gluteraldehyde, 100 mM KCl, 3 mM $MgCl_2$, 10 mM Hepes, 150 mM sucrose, and 0.1% Triton X-100, pH 7.6. Embryos were rinsed three times in PBS, and then animal cap explants were dissected using a scalpel. Animal caps were blocked in Super Block (Pierce) containing 0.1% Triton X-100 for 6–8 h and then were incubated overnight with primary antibodies in blocking buffer at 4 °C. Primary antibodies against C-terminally phosphorylated Smad1 (9511; Cell Signaling Technologies) (dilution 1:100) and Smad2/3 (610842; BD Transduction Labs) (dilution 1:100) were used. Animal caps then were washed four times for 45 min each wash with PBS, 0.2% Triton X-100, incubated overnight at 4 °C with secondary antibodies (Alexa 647) (dilution 1:250 in blocking buffer), and washed three times for 45 min each wash in PBS, 0.2% Triton X-100.

Gene Expression Analysis. C2C12 cells were grown in 6-cm dishes. RNA was collected with the TRIzol reagent (Invitrogen) and was treated with DNase (Ambion), and cDNA was synthesized with the First Strand cDNA synthesis kit (Roche). In all cases, gene expression was normalized to the expression of mHPRT. Primer sequences for mHPRT, mPai1, mSmad7, and mSnail1 were as in Varelas et al. (22). Primer sequences for mSmad2 were forward primer 5′-TACATCCCAGAAACACCACCACCT-3′, reverse primer 5′-ACACCAGAATGCAGGTTCCGAGTA-3′. All experiments were performed at least twice in both the parental and GFP-Smad4 cell lines.

Luciferase Assays. *Xenopus* embryos were injected at the two- or four-cell stage with 15 pg of XVent-luc reporter plasmid per cell. At stage 11, four embryos were lysed together in 50 μL of passive lysis buffer (Promega), and the luciferase assay was performed using the Promega luciferase assay system according to the manufacturer's instructions. C2C12 cells were transfected with 3.6 μg of either 3TP-luc or CAGA12-luc plasmids and 0.4 μg of pRL-Tk for normalization. Cells were treated with TGF-β1 48 h after transfection andwere lysed and analyzed for luciferase activity using the Dual Luciferase Reporter Assay System (Promega) according to the manufacturer's instructions.

Western Blotting. Cells were grown until almost confluent and then were stimulated with TGF-β1. Cells were lysed in cell lysis buffer (Cell Signaling Technologies) containing protease and phosphotase inhibitors, and Western blotting was performed using standard techniques. Antibodies against C-terminally phosphorylated Smad2 (3108; Cell Signaling Technologies) (dilution 1:1,000), Smad2/3 (610482; BD Transduction Labs) (dilution 1:1,000), and Smad4 (B-8; Santa Cruz) (dilution 1:500) were used. In the cell fractionation experiments, nuclei and cytoplasmic extracts were prepared using the NE-PER kit (Pierce) according to the manufacturer's instructions.

Mathematical Modeling. The model in Fig. S6*A* can be translated into the following set of ordinary differential equations.

$$\frac{dR}{dt} = k_{bR} + k_{LR}L - d_R R \qquad \textbf{[S1]}$$

$$\frac{dX}{dt} = k_{bX} + k_{LX}L - d_X X \qquad \textbf{[S2]}$$

$$\frac{dS_4}{dt} = \frac{k_a({S_4}^T - S_4)}{K_a + ({S_4}^T - S_4)} - \frac{k_i X S_4}{K_i + S_4} \qquad \textbf{[S3]}$$

where L denotes the ligand, R denotes the R-Smad, X denotes the postulated negative feedback component, and S_4 denotes nuclear Smad4. In the core model, we assume that the ligand level is fixed, and thus L is a parameter of the model. k_{bi} denotes the basal rate to produce component i, k_{Li} is the rate of induction of i by the ligand, d_i is the rate of degradation for component i, k_i (K_i) and k_a (K_a) are the rates (Michaelis constants) for activation and inactivation of Smad4. In Eq. **S3**, we have made use of the conservation of the

total amount of Smad4. Note that as long as $k_{Li}L \gg k_{bi}$ for $i = R,X$, then the steady-state levels of both R and X are proportional to L, and the steady-state level of S_4 is independent of L; thus Smad4 activation at steady state is independent of ligand level.

To put the ligand under the control of active Smad4, we assumed a simple linear relationship.

$$\frac{dL}{dt} = k_{bL} + aS_4 - d_L L \qquad \textbf{[S4]}$$

This equation together with Eqs. **S1**–**S3** readily generated a system with a Hopf bifurcation that resulted in limit cycle oscillations.

To simulate the cycloheximide experiments, we note that the induction of X is dependent on new transcription, so in the presence of cycloheximide, $k_{LX} = 0$. We also simulated the decay of activated R-Smad at longer times (Fig. 4*C*) by replacing Eq. **S1** with slow exponential decay $\mathrm{dR/dt} = -d_{chx}R$ at times greater than 6 h.

Parameters for the basic model are $k_{bR} = 0, k_{bX} = 0.005, k_{LR} = 1$, $k_{LX} = 0.1$, $k_{dR} = 1$, $k_{dX} = 0.1$, k_a=$k_i = 1$, K_a=$K_i = 0.1$, $S_4^T = 1$. For the oscillating model, the additional parameters are $k_{bL} = 0.1$, $a = 0.5$, $d_L = 1$. For the cycloheximide simulation, we took $d_{chx} = 0.005$.

1. Francois P, Despierre N, Siggia ED (2012) Adaptive temperature compensation in circadian oscillations. *PLoS Comp Biol*, in press.
2. Goldbeter A, Koshland DE, Jr. (1981) An amplified sensitivity arising from covalent modification in biological systems. *Proc Natl Acad Sci USA* 78:6840–6844.
3. Liu F, Pouponnot C, Massagué J (1997) Dual role of the Smad4/DPC4 tumor suppressor in TGFbeta-inducible transcriptional complexes. *Genes Dev* 11:3157–3167.
4. Pierreux CE, Nicolás FJ, Hill CS (2000) Transforming growth factor beta-independent shuttling of Smad4 between the cytoplasm and nucleus. *Mol Cell Biol* 20:9041–9054.
5. Inman GJ, Nicolás FJ, Hill CS (2002) Nucleocytoplasmic shuttling of Smads 2, 3, and 4 permits sensing of TGF-beta receptor activity. *Mol Cell* 10:283–294.
6. Biondi CA, et al. (2007) Mice develop normally in the absence of Smad4 nucleocytoplasmic shuttling. *Biochem J* 404:235–245.
7. Dai F, Lin X, Chang C, Feng X-H (2009) Nuclear export of Smad2 and Smad3 by RanBP3 facilitates termination of TGF-beta signaling. *Dev Cell* 16:345–357.
8. Gao S, et al. (2009) Ubiquitin ligase Nedd4L targets activated Smad2/3 to limit TGF-beta signaling. *Mol Cell* 36:457–468.
9. Lin X, et al. (2006) PPM1A functions as a Smad phosphatase to terminate TGFbeta signaling. *Cell* 125:915–928.
10. Zi Z, et al. (2011) Quantitative analysis of transient and sustained transforming growth factor-β signaling dynamics. *Mol Syst Biol* 7:492.
11. Simeoni I, Gurdon JB (2007) Interpretation of BMP signaling in early Xenopus development. *Dev Biol* 308:82–92.
12. Bourillot P-Y, Garrett N, Gurdon JB (2002) A changing morphogen gradient is interpreted by continuous transduction flow. *Development* 129:2167–2180.
13. Batut J, Howell M, Hill CS (2007) Kinesin-mediated transport of Smad2 is required for signaling in response to TGF-beta ligands. *Dev Cell* 12:261–274.
14. Lacoste A, Berenshteyn F, Brivanlou AH (2009) An efficient and reversible transposable system for gene delivery and lineage-specific differentiation in human embryonic stem cells. *Cell Stem Cell* 5:332–342.
15. Hata A, et al. (2000) OAZ uses distinct DNA- and protein-binding zinc fingers in separate BMP-Smad and Olf signaling pathways. *Cell* 100:229–240.
16. Suzuki A, Shioda N, Ueno N (1995) Bone morphogenetic protein acts as a ventral mesoderm modifier in early Xenopus embryos. *Dev Growth Differ* 37: 581–588.
17. Alarcón C, et al. (2009) Nuclear CDKs drive Smad transcriptional activation and turnover in BMP and TGF-beta pathways. *Cell* 139:757–769.
18. Inman GJ, et al. (2002) SB-431542 is a potent and specific inhibitor of transforming growth factor-beta superfamily type I activin receptor-like kinase (ALK) receptors ALK4, ALK5, and ALK7. *Mol Pharmacol* 62:65–74.
19. Sive HL, Grainger RM, Harland RM (2000) *Early Development of Xenopus laevis: A Laboratory Manual* (Cold Spring Harbor Laboratory, Cold Spring Harbor, NY).
20. Sbalzarini IF, Koumoutsakos P (2005) Feature point tracking and trajectory analysis for video imaging in cell biology. *J Struct Biol* 151:182–195.
21. Larabell CA, et al. (1997) Establishment of the dorso-ventral axis in Xenopus embryos is presaged by early asymmetries in beta-catenin that are modulated by the Wnt signaling pathway. *J Cell Biol* 136:1123–1136.
22. Varelas X, et al. (2010) The Crumbs complex couples cell density sensing to Hippo-dependent control of the TGF-β-SMAD pathway. *Dev Cell* 19:831–844.

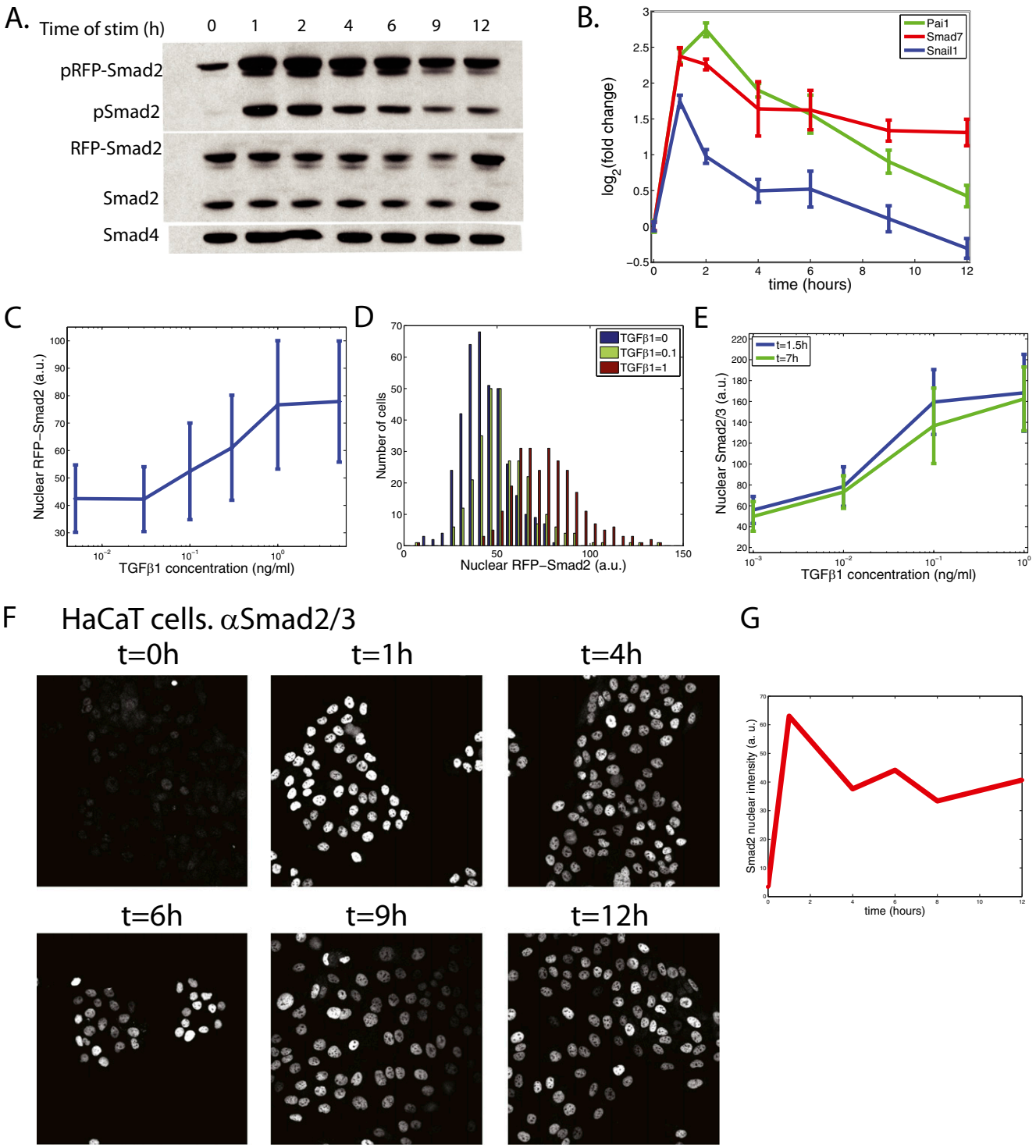

Fig. S1. Signaling activity is not perturbed in the C2C12-RFP-Smad2 cell line, and Smad2/3 activation is graded, homogenous, and stable in C2C12 and HaCaT cells. (*A*) Western blotting analysis of the RFP-Smad2 cell line. Cells were treated for the indicated times with 5 ng/mL TGF-β1, and then total cell lysates were extracted and analyzed by Western blotting. The level of RFP-Smad2 is comparable to the levels of the endogenous protein. (*B*) Quantification of TGF-β1 target genes by quantitative RT-PCR (qRT-PCR) shows that the dynamics of gene expression are comparable to those of the parental cell line (compare with Fig. 2*B* of the main text). (*C*) Quantification of average level of nuclear RFP-Smad2 as a function of ligand level. Error bars show the SD across individual cells and therefore give a measure of the cell-to-cell variability. (*D*) Distributions of nuclear RFP-Smad2 in populations of cells treated with the indicated doses of TGF-β1 showing a graded response. (*E*) Dose–response of endogenous Smad2/3 as detected by immunofluorescence. (*F*) Dynamics of endogenous Smad2/3 by immunofluorescence in HaCaT cells. Cells were fixed at the indicated times after treatment with 2 ng/mL TGF-β1 and were stained with αSmad2/3 antibody. (*G*) Quantification of nuclear Smad2/3 from immunofluorescence images of HaCaT cells. Cells also were stained with Sytox, and nuclei were identified based on the Sytox image. The amount of Smad protein inside the nucleus of each cell was quantified and then averaged over cells. Smad2/3 is detected only in the nucleus after TGF-β1 treatment and persists for the duration of our measurement but with somewhat decreasing intensity.

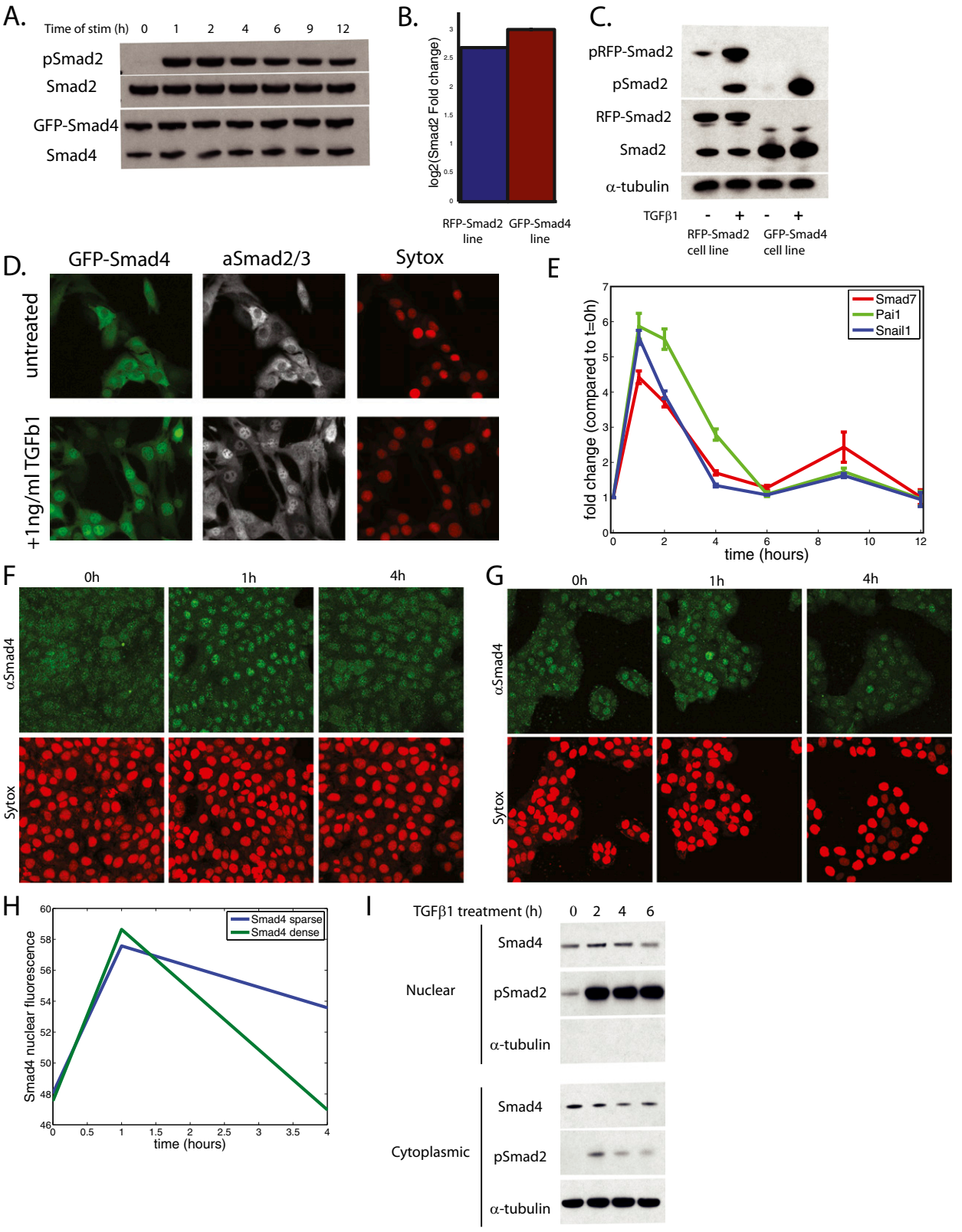

Fig. S2. C2C12-GFP-Smad4 responds normally to signaling, and nuclear localization of endogenous Smad4 is transient in HaCaT cells. (*A*) Western blot analysis of the GFP-Smad4 cell line. Cells were treated for the indicated times with 5 ng/mL TGF-β1, and then total cell lysates were extracted and processed for Western blotting. The dynamics of C-terminal phosphorylation of Smad2 are similar to those of the unmodified cell line (compare with Fig. 1*F*), and GFP-Smad4 is expressed comparably to endogenous Smad4. (*B*) qRT-PCR comparing the level of Smad2 overexpression at the mRNA level in the GFP-Smad4 and the RFP-Smad2 cell lines. Smad2 is overexpressed to a similar extent in the two cell lines. Fold changes are compared with expression in unmodified C2C12 cells. (*C*) Western blot analysis comparing the levels of Smad2 and pSmad2 in the GFP-Smad4 and RFP-Smad2 cell lines. The total amount of Smad2 protein in RFP-Smad2

Legend continued on following page

cell line (RFP-Smad2 and Smad2 combined) is similar to the amount of Smad2 in the GFP-Smad2 cell line, and both lines responded similarly to stimulation with TGF-β1 (5 ng/mL for 1 h). (*D*) Smad2 translocates to the nucleus in GFP-Smad4 cells. Cells were left untreated or were stimulated with 1 ng/mL TGF-β1 for 1 h and then were fixed. Immunofluorescent staining was performed with antibody against Smad2/3 (compare with Fig. 1*E*). Note that because of the overexpression, at the same dose of TGF-β1, more Smad2 remains in the cytoplasm in the overexpressing line; however, the total amount of Smad2/3 that translocates to the nucleus is similar in the two cell lines. (*E*) Induction of target genes is normal in the GFP-Smad4 cell line. Analysis of pathway targets by qRT-PCR (compare with Fig. 2*B*). (*F*) Dynamics of Smad4 nuclear localization by immunofluorescence in dense regions of HaCaT cell cultures. Cells were fixed at the indicated times after the addition of 2 ng/mL TGF-β1 and were stained with an antibody against Smad4. (*G*) As in *A*, except images show sparse regions of the culture dishes shown in *A*. (*H*) Quantification of nuclear Smad4 dynamics from the immunofluorescence images showing a more sustained response in low-density cultures. (*I*) Dense cultures of HaCaT cells were fractionated into nuclear and cytoplasmic compartments and were analyzed by Western blotting. Nuclear Smad4 decreases at 6 h, whereas nuclear pSmad2 is sustained.

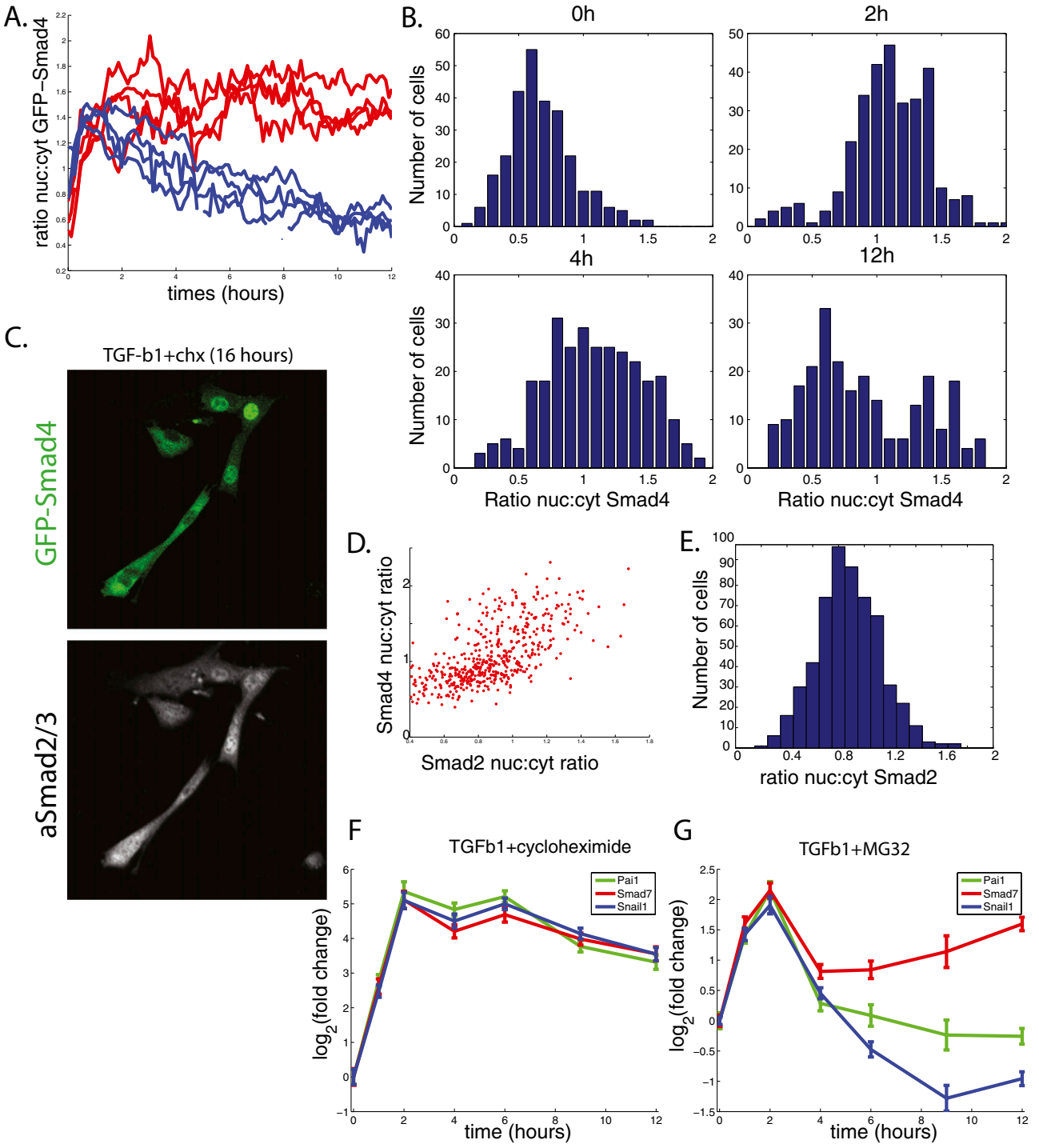

Fig. S3. GFP-Smad4 localization is binary and correlates with Smad2 activation in cycloheximide-treated C2C12 GFP-Smad4 cells. Transcriptional dynamics with TGF-β1 and either cycloheximide or MG132 are nearly identical in the parental and GFP-Smad4 cell lines. (*A*) Dynamics of Smad4 localization in single cells treated with TGF-β1 (5 ng/mL) and cycloheximide (50 μg/mL). (*B*) Histograms of the ratio of nuclear to cytoplasmic GFP-Smad4 concentration at the times indicated. All cells respond initially, but only a subset of the population has a sustained response. (*C*) In populations with binary Smad4 response, Smad4 localization correlates with Smad2. GFP-Smad4 cells were treated with TGF-β1 and cycloheximide for 16 h and then were fixed and analyzed by immunofluorescence for Smad2/3 localization. (*D*) Scatterplot obtained under the same conditions as *C* comparing nuclear with cytoplasmic ratios of Smad2 and Smad4. (*E*) Histogram of Smad2 nuclear-to-cytoplasmic ratios. The Smad2 population does not exhibit a binary response. (*F* and *G*) Unmodified C2C12 cells were treated with TGF-β1 (5 ng/mL) and either cycloheximide (50 μg/mL) (*F*) or MG132 (10 μM\) (*G*), and target gene expression was analyzed by qRT-PCR. Compare with the C2C12 GFP-Smad4 cell line presented in Fig. 4 *D* and *E*.

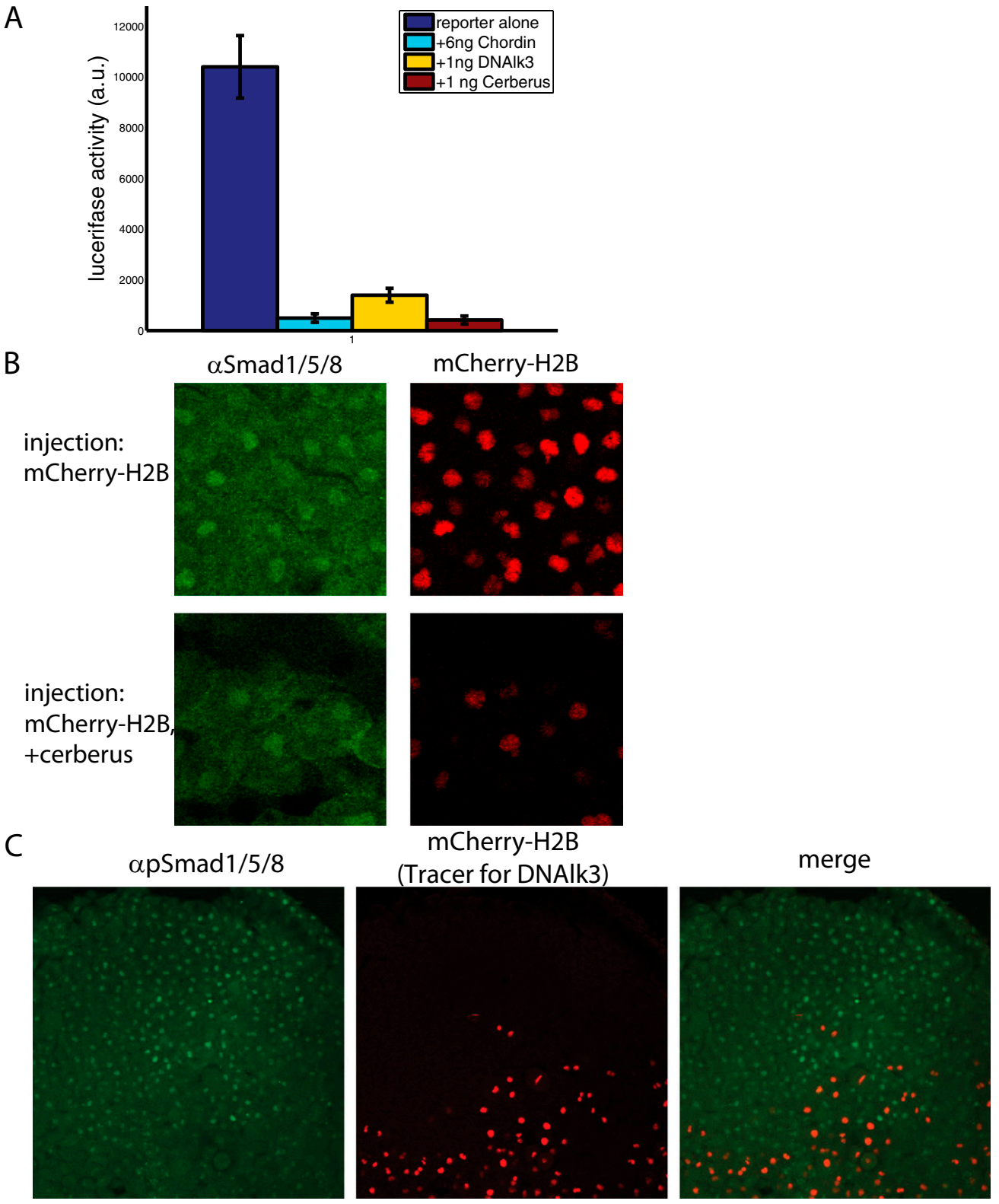

Fig. S4. Inhibition of BMP signaling reduces pSmad1/5/8 and transcription from the XVent2 promoter but does not alter Smad1 localization in *Xenopus* ectodermal tissue. (*A*) Embryos at the two-cell stage were injected with XVent2-luc reporter and the indicated mRNA. At gastrula stage (stage 11), embryos were lysed and analyzed for luciferase activity. (*B*) Embryos at the two-cell stage were injected with the indicated mRNA into each cell. At stage 9, embryos were fixed, and animal caps were dissected and analyzed by immunofluorescence for Smad1/5/8. Although the total fluorescence is reduced in the Cerberus-injected animal cap, the ratio of nuclear to cytoplasmic Smad1 remained nearly the same. (*C*) Embryos at the two-cell stage were injected in one cell with mRNA encoding DNAlk3 and mCherry-H2B. At stage 9, embryos were fixed, and animal caps were dissected and analyzed for pSmad1/5/8 by immunofluorescence. Cells receiving DNAlk3 have reduced nuclear pSmad1/5/8.

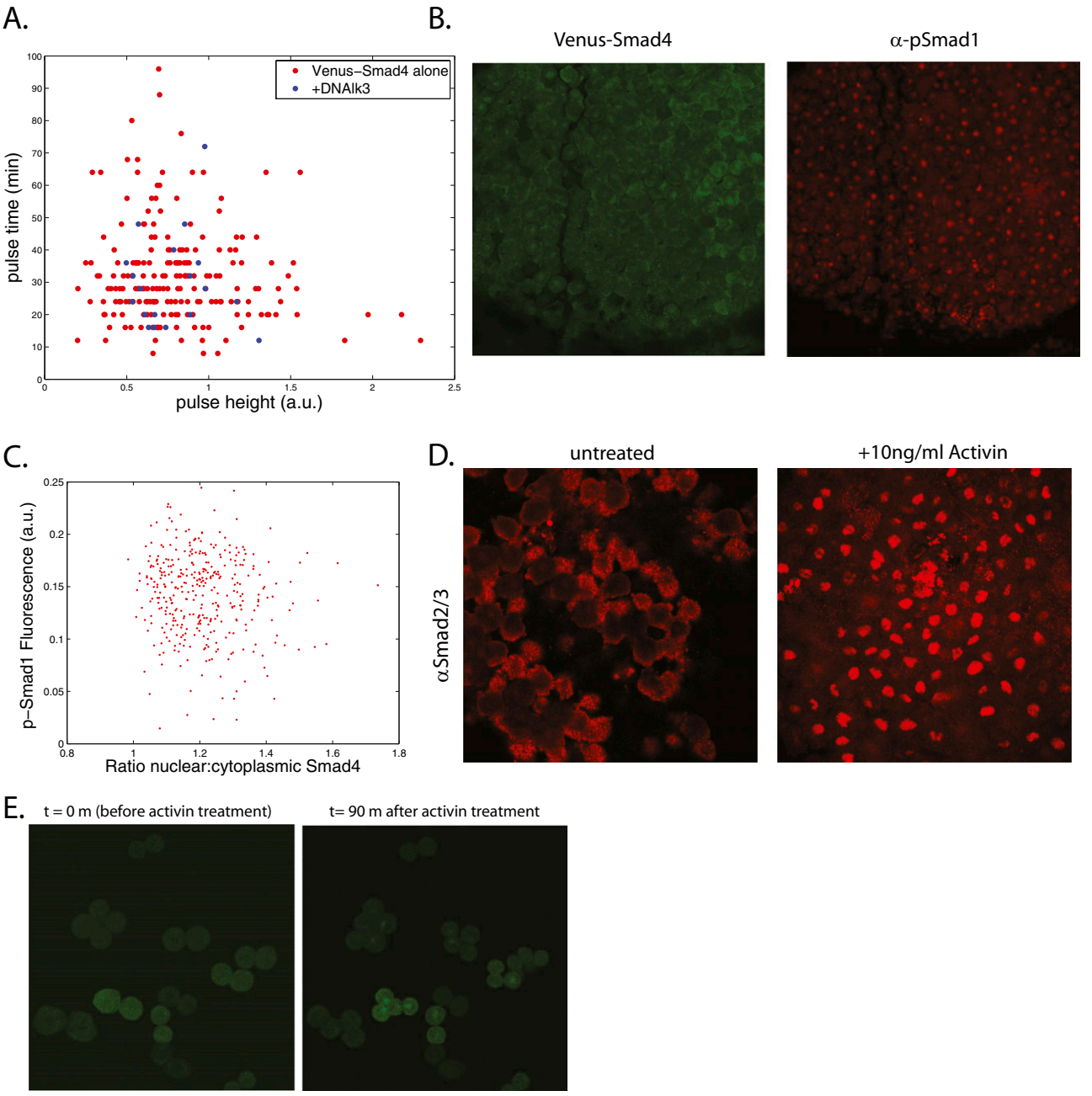

Fig. S5. Inhibition of BMP signaling reduces the number of bursts but does not affect the character of the remaining bursts. Smad1 and Smad2 activation is homogenous in the animal cap and is uncorrelated with Smad4. (*A*) Scatterplot of pulse heights and times for embryos injected with Venus-Smad4 alone or with Venus Smad4 and DNAlk3. (*B*) Embryos were injected in the animal pole at the two-cell stage with mRNA encoding a Venus-Smad4 fusion protein. At stage 9, the embryos were fixed, and animal caps were dissected and stained with an antibody against C-terminally phosphorylated Smad1/5/8, which responds to the endogenous BMP4 ligand. (*C*) Quantification of fluorescence from the image in *B*. (*D*) Animal cap explants were dissected at stage 9 and cultured in low-calcium medium either with or without 10 ng/mL activin for 30 min. Explants then were fixed and analyzed by immunofluorescence with an antibody against Smad2/3. (*E*) Embryos were injected in the animal pole at the two-cell stage with mRNA encoding Venus-Smad4. Animal cap explants were dissected at stage 9 to eliminate the BMP response, and cells were dissociated in calcium- and magnesium-free medium. Activin (10 ng/mL) was added, and images were taken at the indicated times.

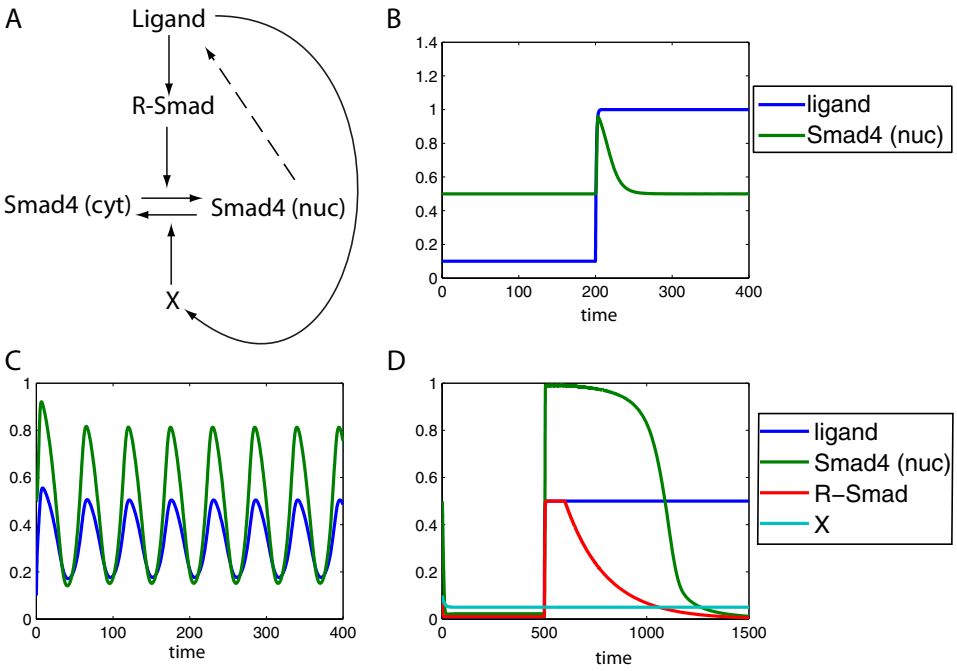

Fig. S6. Mathematical modeling shows a connection between adaptive and oscillatory/pulsing behaviors. (*A*) Schematic of interactions included in the model. The dashed line shows the additional feedback that will cause the system to become oscillatory. This schematic model was translated into ordinary differential equations as described in *SI Materials and Methods*. (*B*) The model exhibits adaptive behavior in nuclear Smad4 in response to a step increase in ligand concentration. (*C*) Addition of feedback from nuclear Smad4 to the ligand results in oscillatory behavior. (*D*) Model explains long-term bistability when the induction of X by the ligand is blocked by cycloheximide and a slow decay of the R-Smad is added. The ratio of R-Smad to X will determine whether a cell is on or off.

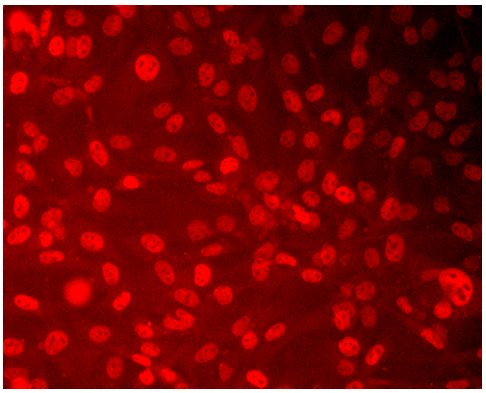

Movie S1. RFP-Smad2 stably accumulates in the nucleus. This movie was quantified in Fig. 1*D*. Cells from the RFP-Smad2 cell line were treated with 5 ng/mL TGF-β1 immediately after the first image was taken. Movie duration is 12 h, and images were collected every 8 min.

Movie S1

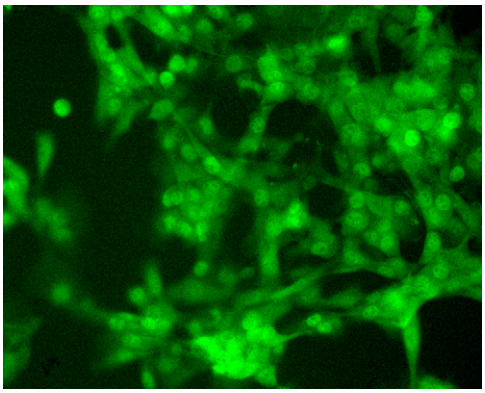

Movie S2. GFP-Smad4 transiently accumulates in the nucleus. This movie was quantified in Fig. 3*C*. GFP-Smad4 cells were treated with 5ng/mL TGF-β1 immediately after the first image was taken. Movie duration is 8 h, and images were collected every 6 min.

Movie S2

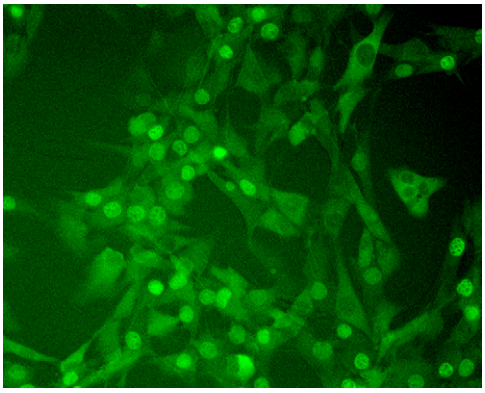

Movie S3. Cycloheximide prolongs the duration of GFP-Smad4 nuclear localization. This movie was quantified in Fig. 4*B*. GFP-Smad4 cells were pretreated with cycloheximide for 30 min before the first image was taken. Immediately after the first image was taken, 5 ng/mL TGF-β1 was added. Movie duration is 14 h, and images were collected every 7 min.

Movie S3

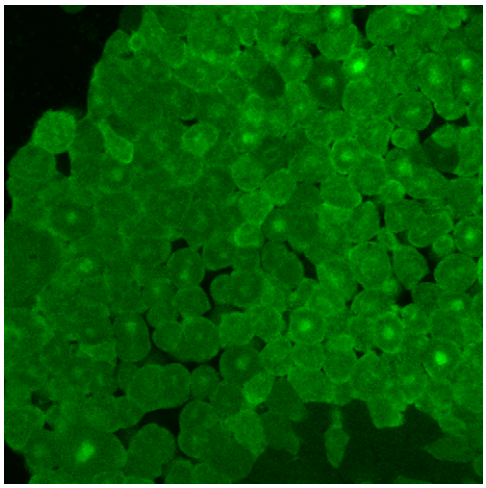

Movie S4. Smad4 enters the nucleus in brief bursts in *Xenopus* animal cap explants. Snapshots from this movie are shown in Fig. 5*D*. At the two-cell stage, each cell was injected in the animal pole with Venus-Smad4 and mCherry-H2B. At stage 9, the animal pole was dissected and cultured on fibronectin-coated glass. Movie duration is 2.5 h, and images were collected every 3 min. The image shown in the movie is a maximum intensity projection of the z-planes containing most of the nuclei.

Movie S4

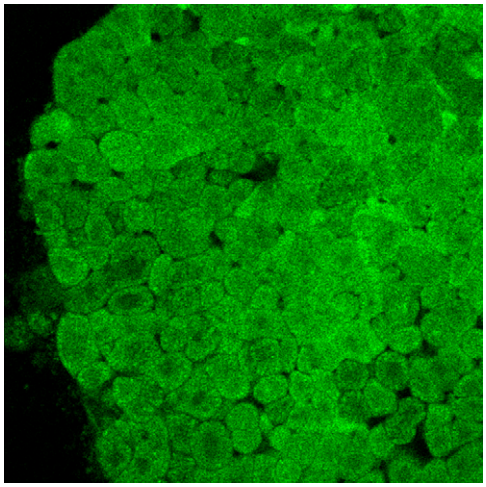

Movie S5. Smad4 bursts are dependent on BMP signaling. A snapshot from this movie is shown in Fig. 6*A*. The conditions in this movie are the same as Movie S4, except that 1 ng DNAlk3 also was injected into each cell of the embryo. The animal cap explant was taken from a sibling embryo of the embryo used to make the explant for Movie S4. Movie duration is 2.5 h, and images were collected every 3 min. The image shown in the movie is a maximum intensity projection of the z-planes containing most of the nuclei.

Movie S5

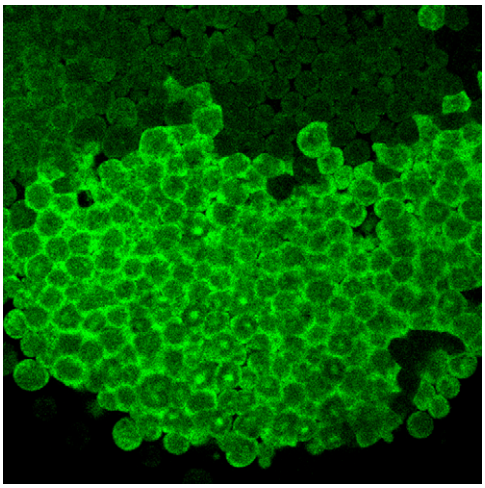

Movie S6. Smad4 bursts can be restored by activin treatment following BMP inhibition. A snapshot from this movie is shown in Fig. 6*D*. Conditions are as in Movie S5, except that 10 ng/mL activin was added immediately before the start of the movie. Movie duration is 2 h, and images were collected every 2.5 min.

Movie S6